Dynamically adjusted cell fate decisions and resilience to mutant invasion during steady-state hematopoiesis revealed by an experimentally parameterized mathematical model

Natalia L. Komarova^{1*}, Chiara Rignot², Angela G. Fleischman³ & Dominik Wodarz^{4*}

- 1: Department of Mathematics, University of California San Diego, 9500 Gilman Drive, La Jolla, CA 92093
- 2: Department of Mathematics, University of California Irvine, Irvine CA 92697, USA
- 3: Department of Medicine, University of California Irvine, Irvine CA 92697, USA
- 4: Department of Ecology, Behavior & Evolution, University of California San Diego, 9500 Gilman Drive, La Jolla CA 92093, USA

^{*} corresponding authors

Abstract

A major next step in hematopoietic stem cell (HSC) biology is to enhance our quantitative understanding of cellular and evolutionary dynamics involved in undisturbed hematopoiesis. Mathematical models have been and continue to be key in this respect. and are most powerful when parameterized experimentally and containing sufficient biological complexity. In this paper, we use data from label propagation experiments in mice to parameterize a mathematical model of hematopoiesis that includes homeostatic control mechanisms as well as clonal evolution. We find that non-linear feedback control can drastically change the interpretation of kinetic estimates at homeostasis. This suggests that short-term HSC and multipotent progenitors (MPPs) can dynamically adjust to sustain themselves temporarily in the absence of long-term HSCs, even if they differentiate more often than they self-renew in undisturbed homeostasis. Additionally, the presence of feedback control in the model renders the system resilient against mutant invasion. Invasion barriers, however, can be overcome by a combination of agerelated changes in stem cell differentiation and evolutionary niche construction dynamics based on a mutant-associated inflammatory environment. This helps us understand the evolution of e.g. TET2 or DNMT3A mutants, and how to potentially reduce mutant burden.

Significance statement

The maintenance of the hematopoietic system is a complex process where different types of stem cell divisions are regulated by homeostatic control networks. A mathematical model, parameterized with detailed mouse data, is used to capture this complexity. We investigate conditions under which advantageous mutants emerge. The model predicts a mutant invasion barrier in cell populations where mutants are most likely generated (e.g. progenitor cells), requiring mutants to have a large fitness advantage. It further suggests that age-related changes in the stem cell dynamics can promote mutant invasion, especially if mutants generate a favorable environment for themselves (evolutionary niche construction). This has relevance for understanding and managing the growth of TET2 and DNMT3A mutants, which are associated with chronic health conditions.

1. Introduction

The biology of hematopoietic stem cells has been subject to much investigation, and an increasingly detailed picture has been emerging, which includes the hierarchical structure of the hematopoietic system (1), the mechanisms underlying the associated cell fate decisions (2-6), and the kinetics of these processes (7-14). At the same time, it has become clear that the dynamics within the hematopoietic system are characterized by complex interactions among cells, involving homeostatic control mechanisms (15, 16). Further complexity is added through evolutionary processes (17-19), resulting in the emergence of specific cell clones that can potentially increase the risk of subsequent malignant transformation and also trigger a number of non-malignant chronic health conditions (20). Mathematical models have been used to parse the complexity of the interactions occurring within the hematopoietic system, and to investigate the principles according to which mutant cell clones emerge and give rise to tumors (21-37).

Building mathematical models of the hematopoietic system has been a large-scale continuous effort with a wealth of results contributed by many groups around the world. Starting with pioneering work by Mackey, Loeffler, Roeder and colleagues in the early 2000s and before (32, 38-43), HSC modeling has gained further complexity and sophistication in the following decades, including a focus on non-linear control mechanisms (21-31, 33-37, 44-49). Among major contributions are models by Marciniak-Czochra, Stiehl and colleagues who have created a mathematical foundation for the dynamics of hematopoiesis (11, 21, 23, 50-53); further significant efforts included the studies of leukemias and other hematopoietic disorders in the context of cell evolution and drug treatments (22, 36, 37, 54-65). Many of these models were calibrated based on the experimental information that was available at the time. With the advances of experimental techniques, the ability to parameterize models of different degrees of complexity has been continuously improving. A major breakthrough came with the neutral label propagation data made available by Busch et al (7). These data have recently informed mathematical models in select settings (66, 67). In the current

paper, we provide the next step, which bridges between homeostatic cell regulation and evolution. Specifically, we use neutral label propagation data to parameterize a model of hematopoiesis at homeostasis that contains both non-linear homeostatic control mechanisms and cellular evolutionary dynamics. This results in new insights that allow a more comprehensive interpretation of kinetic data resulting from the label propagation studies, and identifies evolutionary barriers to mutant emergence that indicate resilience against mutant invasion during homeostasis. The model further identifies mechanisms that enable mutant cells to overcome these invasion barriers, based on evolutionary niche construction and age-related changes.

2. Model-based interpretation of estimated self-renewal rates of ST-HSCs and MPPs.

Our analysis is based on a mathematical model of hematopoiesis that has been extensively used in the literature (21-37), illustrated in Figure 1 and given by a set of ordinary differential equations that describe the dynamics of cell populations over time. We explicitly describe the dynamics of LT-HSCs (x_0), ST-HSCs (x_1), and MPPs (x_2). These cells are assumed to divide with a rate r_i . A division is assumed to result in self-renewal (two daughter stem cells) with a probability p_i , and in differentiation (two daughter downstream cells) with a probability $1-p_i$. We also include populations of common myeloid progenitor (CMP, $x_3^{(1)}$) and common lymphoid progenitor (CLP, $x_3^{(2)}$) cells.

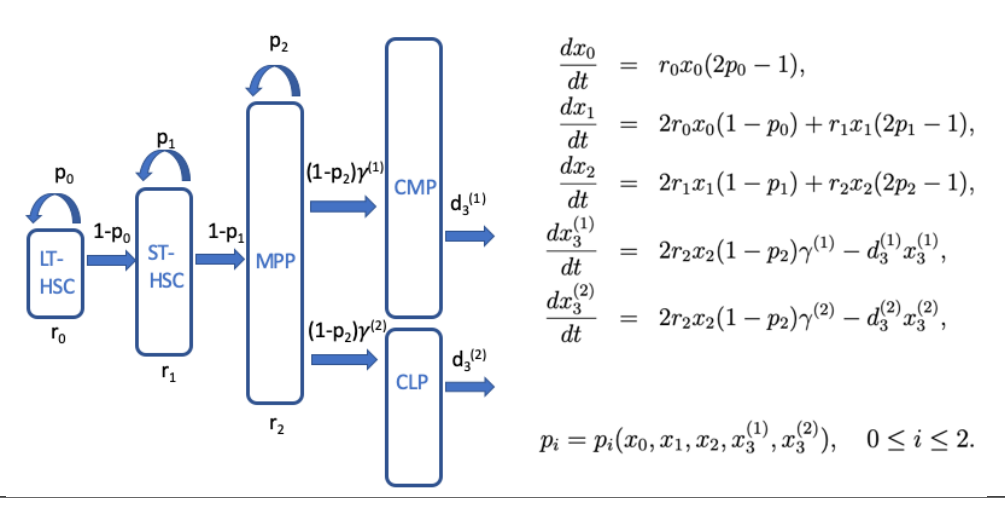


Figure 1: A schematic of the mathematical model showing the four compartments and the associated division rates and self-renewal probabilities. The system of ordinary differential equations used to describe the dynamics is provided on the right.

This model is parameterized with the help of existing neutral label propagation data in mice at homeostatic setpoint, first published by Busch et al (7), and expanded with additional data in a subsequent study (68). There, 1% of LT-HSCs was labeled, and the progression of the neutral label in ST-HSCs, MPPs, CMPs, and CLPs was documented for about 450 days. The model was fit to these data as described in the SI Appendix, and the best fitting parameters as well as their confidence intervals are given in Table 1. The fits and the data are presented in SI Figure S2. A similar model fitting approach was taken to estimate parameters by Busch et al (7), but the model we use is structurally different (due to our focus on evolutionary dynamics), thus necessitating the parameter estimation procedures performed here.

We will first briefly consider the scenario where the estimated parameters are constants. We subsequently examine the dynamics under the assumption that the estimated parameters (in particular, the cells' probability of self-renewal) at homeostasis are subject to feedback control.

Notation	Parameter definition	Value	95% C.I.	Units
r_0	Division rate of LT-HSCs	0.0107	(0.0084, 0.014)	days ⁻¹
r_1	Division rate of ST-HSCs	0.067	(0.021,0.10)	days ⁻¹
r_2	Division rate of MPPs	0.136	(0.066, 0.95)	days ⁻¹
$ar{p}_0$	Self-renewal probability of LT-HSCs	0.5		1
$ar{p}_1$	Self-renewal probability of ST-HSCs	0.473	(0.40, 0.48)	1
$ar{p}_2$	Self-renewal probability of MPPs	0.416	(0.323,0.49)	1
$d_3^{(1)}$	Removal rate of CMPs	0.034	(0.017,0.22)	days ⁻¹
$d_3^{(2)}$	Removal rate of CLPs	0.007	(0.005,0.017)	days ⁻¹
\bar{x}_0	Equilibrium number of LT-HSCs	17,000*		cells

Table 1: Definitions of model parameters and their values. The bar over values $\overline{p_i}$ and $\overline{x_0}$ is used to indicate that these are constants, and to distinguish these from functions $p_i(x_0,...)$ and $x_0(t)$. * There is a degree of uncertainty about the number of LT-HSCs (7), but none of the qualitative results depend on this value: all the values simply scale with the number of LT-HSCs and a change in this value would result in a multiplicative factor.

2.1 Constant parameter values

In the most basic setting, we can assume that the rate of cell division and self-renewal at homeostasis are constants, "programmed" into the cells. Hence, we can use the estimated parameter values to simply set $p_i = \bar{p}_i$ (Table 1). Note that the self-renewal probability of LT-HSCs was set to be \bar{p}_0 =0.5, because in this type of model without feedback, this is the only way in which a homeostatic population is maintained at equilibirum (p_0 >0 leads to exponential cell growth, while p_0 <0.5 leads to extinction, see SI Section 1). The self-renewal rates of the downstream compartments were estimated by model fitting and are both below one half (\bar{p}_1 =0.472, \bar{p}_2 =0.416). Under the current assumptions, this means that the ST-HSC and the MPP compartments cannot maintain themselves, and that their persistence strictly depends on the input from the LT-HSCs. This has also been the conclusion of (7).

2.2. Parameter values are determined by feedback control at homeostasis

An alternative, and biologically more complex assumption is that the observed equilibrium rates of cell division and self-renewal are maintained dynamically through

feedback control mechanisms. Experimental data indicate that both the rate of cell division, r_i , and the probability of self-renewal, p_i , might be subject to feedback control, because these processes seem to accelerate during tissue reconstitution compared to homeostatic setpoint (7). Here we assume that the self-renewal probability, p_i , of LT-HSCs, ST-HSCs, and MPPs can be influenced by feedback regulation. For simplicity, we continue to treat the division rate of cells, r_i , as constants. The reason is that in the current study we focus on dynamics at homeostasis, and in this context, only assumptions about the self-renewal probability of cells have an impact on the stability properties of the model (69).

Modeling feedback control: Since the exact functional form of feedback on the self-renewal probability, p_i , is not known, different possibilities have been explored in the literature. For example, in previous studies (21-23) it was assumed that the final, most differentiated cell population reduces the self-renewal probability of cells (importantly p_0), which then results in the presence of stable equilibria. There are many other possible ways in which the self-renewal probability of cells could be regulated. We could write in general that in compartment i, the probability of self-renewal of cells is some function of cell populations in the same and other compartments: $p_i = p_i(x_0, x_1, x_2, x_3)$. At healthy, homeostatic equilibrium, the value of this function is assumed to be equal to the experimentally measured self-renewal probability, \bar{p}_i (Table 1).

Here, we explore how the interpretation of the estimated self-renewal probabilities can change if we assume that homeostasis is driven by feedback control. In the SI Appendix, we provide calculations using different types of control. We show that results reported here hold true generally, for a large class of feedback regulation functions that satisfy some mild conditions (such as the existence of a stable equilibrium). Here, for illustration purposes, we will discuss results in the context of one specific feedback loop, where homeostasis is maintained by feedback of LT-HSCs on their own self-renewal probability, p_0 , and similar feedback by populations of the downstream compartments on their own self-renewal probability. Mathematically, this is expressed by assuming that p_0 is a decreasing function of x_0 , for example,

 $p_0=c_0/(h_0x_0+1)$, where c_0 is the LT-HSC self-renewal probability in the absence of feedback, and h_0 is the strength of the feedback regulation. While this alone is sufficient to achieve a stable equilibrium, we will assume that the ST-HSC and MPP cell populations (x_1 and x_2) can potentially limit their own self-renewal probabilities in a similar way, i.e. $p_1=c_1/(h_1x_1+1)$ and $p_2=c_2/(h_2x_2+1)$. While this formulation can correspond to feedback mediated by the cells themselves, it can also be interpreted to represent feedback from the microenvironment, which senses the number of cells.

Model calibration in the presence of feedback: Using our estimated parameters (Table 1), we have p_0 = c_0 /(h_0 X $_0$ +1)=0.5, where X_0 is the LT-HSC population at homeostasis. It has been estimated that a mouse contains approximately 1.7x10⁴ hematopoietic stem cells (7) (our conclusions do not depend on the accuracy of this number, see Table 1 and SI Appendix). For an assumed (and unknown) value of h_0 , which quantifies the amount of regulation that takes place in the system (the higher h_0 , the stronger the control), we determine the value of c_0 such that the LT-HSC population equals $1.7x10^4$. Similarly, setting the values of h_1 and h_2 to a desired level (describing the strength of the control loops for ST-HSCs and MPPs), and using the equations $p_1(x_1) = \bar{p}_1$, $p_2(x_2) = \bar{p}_2$, we can calculate the values of c_1 and c_2 such that the effective self-renewal probabilities at equilibrium matches the experimentally observed ones. The following choices guarantee that at the equilibrium, the self-renewal probabilities coincide with their experimentally measured values for LT-HSCs, ST-HSCs, and MPPs:

$$\begin{array}{rcl} c_0 & = & \frac{1}{2} + \frac{h_0 \bar{x}_0}{2}, \\ \\ c_1 & = & \bar{p}_1 + \frac{r_0 \bar{x}_0 h_1 \bar{p}_1}{r_1 (1 - 2\bar{p}_1)}, \\ \\ c_2 & = & \bar{p}_2 + \frac{2r_0 \bar{x}_0 h_2 (1 - \bar{p}_1) \bar{p}_2}{r_2 (1 - 2\bar{p}_1) (1 - 2\bar{p}_2)}. \end{array}$$

(For calibration under more general assumptions on the feedback function, see SI Section 1). Note that if we set h_i =0 (no control, constant self-renewal probabilities), we simply obtain that the self-renewal probabilities p_0 , p_1 , and p_2 are equal to the experimentally measured values ($p_0 = 1/2$, $p_1 = \bar{p}_1$, $p_2 = \bar{p}_2$).

<u>Can ST-HSCs and MPPs self-maintain?</u> Given that the estimated self-renewal probabilities of ST-HSCs and MPPs are less than one-half (Table 1), the first interpretation that comes to mind is that these populations cannot maintain themselves in the absence of input from the LT-HSC compartment. According to the model with feedback control, however, this need not be the case. Let us consider ST-HSCs as an example. Let us assume that the self-renewal probability of ST-HSC in the absence of negative feedback inhibition, c_1 , is greater than one half. This means that the ST-HSC cell population can maintain itself even without the input from LT-HSCs. At the same time, in the context of our model, the negative feedback will result in an equilibrium value of $p_1 < 0.5$ (and equal to the experimentally measured rate of self-renewal, \bar{p}_1), giving the false impression that this cell compartment cannot persist in the absence of LT-HSCs.

A biological interpretation of the above mathematical statement is as follows. The experimentally measured effective self-renewal probability of ST-HSCs and MPPs $(\bar{p}_1 \text{ and } \bar{p}_2)$ at equilibrium is determined by both (i) the basic division dynamics of the cells in these compartments and (ii) the influx of cells from the upstream compartment. If there is no influx from cells upstream in the differentiation pathway (as is the case for LT-HSCs), the self-renewal probability at equilibrium in the presence of negative feedback is exactly one half, that is, at the population level, half of the cell divisions result in self renewal, and half result in downstream differentiation. The presence of cell influx from an upstream compartment, however, changes this balance, reducing the effective self-renewal probability at equilibrium to a value less than one half. The stronger the cell influx from the upstream compartment, the lower the equilibrium self-renewal probability falls below one half. This is because the influx increases the number of cells in this compartment beyond what division events alone would achieve, thus raising the overall amount of negative feedback.

Since cells now differentiate more often than self-renew, it gives the impression that these cell populations cannot maintain themselves. It follows from our model, however, that if the upstream compartment is removed and the cell influx stops, the cell population that previously differentiated more often than it self-renewed might now effectively act like a stem cell compartment with equal self-renewal and differentiation

rates. This is shown in Figure 2. The simulation starts at homeostasis, where population sizes are at equilibrium and the self-renewal probability of LT-HSCs is one half, while the self-renewal probability of ST-HSCs and MPPs is less than one half, using the estimated parameters (Table 1). At the indicated time point, the LT-HSCs (blue line) are removed in Figure 2A. Consequently, the cell populations adjust but do not go extinct (Figure 2A, top). The self-renewal probability of the ST-HSCs rises to exactly one half (Figure 2A, bottom), because the influx of LT-HSCs due to differentiation has stopped. The self-renewal probability of MPP also increases, but remains below one half, due to

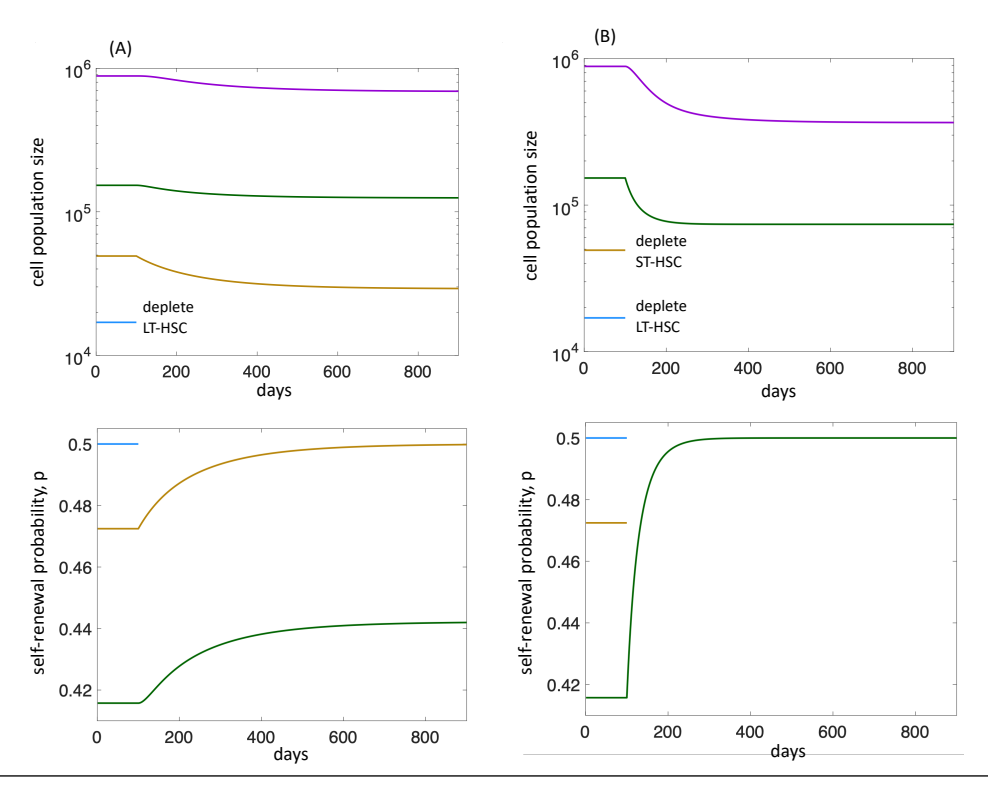


Figure 2. Computer simulation of stem cell depletion. LT-HSCs, ST-HSCs, MPPs, and the sum of CMPs and CLPs are shown in blue, yellow, green, and purple lines. Initially, the system is at homeostatic equilibrium. (A) At 100 days, the LT-HSC population is removed. (B) At 100 days, both the LT-HSCs and the ST-HSCs are removed. We note that this simulation does not include replication limits. If replication limits were included, population extinction would eventually occur when the cells have exhausted their replicative capacity. Negative feedback on the self-renewal probabilities by cells in the same compartment was used, with h_0 =10⁻⁵, h_1 =10^{-5.5}, h_2 =10^{-5.5}. The rest of the parameters are given in Table1.

the continued influx of ST-HSCs. In Figure 2B, the same kind of simulation is repeated, but both LT-HSCs and ST-HSCs are depleted, as indicated. Now, the self-renewal probability of MPPs rises to exactly one half, due to the lack of influx from upstream cell populations, allowing the MPPs to maintain the system.

The same result can be derived for a more general functional form of feedback control (SI Appendix). The important point is that in models with control that are consistent with experimentally measured parameters, compartments that exhibit a self-renewal probability <1/2 may still be able to self-maintain, due to the adjusted increase of this probability in the absence of an upstream compartment.

We note that the ability of these downstream cell populations to "maintain themselves" indefinitely in the absence of LT-HSCs in our model is due to the absence of replication limits in the equations that describe the dynamics of these cell populations. If, however, down-stream cell populations are subject to replication limits (see SI Section 4), maintenance of these cell populations in the absence of LT-HSCs is only temporary. Once their replicative potential is exhausted, the cell populations are predicted to go extinct. These model properties are consistent with experimental data in which ST-HSCs or MPPs can at least temporarily maintain a functional hematopoietic system even if the LT-HSC population is compromised (70-73).

3. Evolutionary Dynamics in the estimated parameter space

Next, we investigate the evolutionary dynamics in this model using the estimated parameters. Denoting wild-type LT-HSCs, ST-HSCs, MPPs and further downstream CMP and CLP cells by x_0 , x_1 , x_2 , $x_3^{(1)}$, and $x_3^{(2)}$, respectively, and the corresponding mutant cells by y_0 , y_1 , y_2 , $y_3^{(1)}$ and $y_3^{(2)}$, the model with feedback control is given by the following set of ODEs:

$$\begin{split} \frac{dx_0}{dt} &= r_0 x_0 (2p_0 - 1), \qquad \frac{dy_0}{dt} = r_0 y_0 (2p_0^{(m)} - 1), \\ \frac{dx_1}{dt} &= 2r_0 x_0 (1 - p_0) + r_1 x_1 (2p_1 - 1), \qquad \frac{dy_1}{dt} = 2r_0 y_0 (1 - p_0^{(m)}) + r_1 y_1 (2p_1^{(m)} - 1), \\ \frac{dx_2}{dt} &= 2r_1 x_1 (1 - p_1) + r_2 x_2 (2p_2 - 1), \qquad \frac{dy_2}{dt} = 2r_1 y_1 (1 - p_1^{(m)}) + r_2 y_2 (2p_2^{(m)} - 1), \\ \frac{dx_3^{(1)}}{dt} &= 2r_2 x_2 (1 - p_2) \gamma^{(1)} - d_3^{(1)} x_3^{(1)}, \qquad \frac{dy_3^{(1)}}{dt} = 2r_2 y_2 (1 - p_2^{(m)}) \gamma^{(1)} - d_3^{(1)} y_3^{(1)}, \\ \frac{dx_3^{(2)}}{dt} &= 2r_2 x_2 (1 - p_2) \gamma^{(2)} - d_3^{(2)} x_3^{(2)}, \qquad \frac{dy_3^{(2)}}{dt} = 2r_2 y_2 (1 - p_2^{(m)}) \gamma^{(2)} - d_3^{(2)} y_3^{(2)} \end{split}$$

Mutant-specific parameters are denoted by superscript (m). WT and mutant cells are assumed to compete with each other through shared feedback control, e.g. the self-renewal probability for WT and mutant LT-HSCs is given by $p_0=c_0/(h_0(x_0+y_0)+1)$ and $p_0^{(m)}=c_0^{(m)}/(h_0^{(m)}(x_0+y_0)+1)$, respectively, and similarly for ST-HSCs and MPPs. We will study the invasion dynamics of an advantageous mutant assuming that it arises in different cell compartments, including LT-HSCs, ST-HSCs, and MPPs. In the above system, de-novo mutations are not included (see SI Section 2 for equations describing continuous mutant generation). Instead, here we investigate the fate of mutants by placing them in different compartments and studying the resulting competition dynamics between wild-type and mutant cells, asking under which conditions the mutant can invade from low numbers.

We focus on advantageous mutants. In general, mutants may have properties different from those of wild-type cells, including an increased replication rate, an increased probability of self-renewal, or an increased replication limit. It has been shown (22, 37, 69) that in models of the type employed here, a mutant whose replication rate is increased (but the probability of self-renewal is unaffected) does not behave as an advantageous mutant. Therefore, in what follows we will assume that mutants' overall replication rate is the same as that of the wild type, but that parameters determining the self-renewal probability differ.

3.1 Invasion barriers for mutants originating in different compartments

<u>LT-HSC compartment:</u> If the mutant emerges in the LT-HSC compartment, the evolutionary dynamics have been investigated previously in a similar model (22, 37). Assume that mutants are characterized by an increased probability of self-renewal. Suppose that the basic probability of self-renewal in the absence of feedback, c_0 , is the only parameter that varies between wild-type and mutant cells, and denote the equivalent mutant parameter by $c_0^{(m)}$. Then the condition for mutant invasion is $c_0^{(m)} > c_0$. The cell population with the larger basic self-renewal probability wins and replaces the competing cell population. Another parameter that determines fitness in our model is

the strength of feedback inhibition of self-renewal, denoted by h_0 in the LT-HSC compartment. If this is the only parameter that varies between WT and mutant cells, then a mutant invades and replaces the wild-type population if $h_0^{(m)} < h_0$. In the most general case, where the mutant self-renewal probability is given by $p_0^{(m)}$, the condition for the mutant winning is given by $p_0^{(m)} > p_0$, where both quantities are measured at the wild-type equilibrium. This straightforward result is consistent with the previous literature (22).

Downstream replicating compartments: If the mutant arises in either the ST-HSC or the MPP compartments, the conditions for mutant invasion are different. Although mutant and WT cells compete with each other in these compartments, the mutant does not necessarily invade if it has a reproductive fitness advantage (e.g., a higher self-renewal probability compared to the wild type). Instead, the reproductive advantage of the mutant needs to be sufficiently large and lie above a threshold for invasion to be successful. Let us suppose that the self-renewal rate of mutants in the ST-HSC compartment differs from that of wild-types by a constant factor: $p_1^{(m)} = (1+s)p_1$, where s is the selection coefficient. The condition for the mutant to succeed (that is, to establish a nonzero presence) in the ST-HSC compartment is given by: $s > s_c^{(1)}$, where $s_c^{(1)} = \frac{1}{2\bar{p}_1} - 1$ (note that this condition is general and does not depend on the specifics of the feedback function, see SI Section 2).

For the parameter values in Table 1, the invasion threshold for the ST-HSC compartment is approximately 0.0582. This means that if a mutant is generated in the ST-HSC compartment, its fitness advantage must exceed 5.82% for those cells to be able to establish a presence among the ST-HSC population, and subsequently invade the downstream compartments. Similarly, if a mutant originates in the MPP compartment, its fitness threshold under parameter values in Table 1 is given by $s_c^{(2)} = \frac{1}{2\bar{p}_2} - 1 \approx 0.203$, that is, fitness advantage must exceed 20.3%. At the same time, note that confidence intervals for the estimates can be relatively large (especially for MPPs),

indicating a degree of uncertainty regarding the exact magnitude of the invasion threshold.

The reason for the threshold behavior is as follows. For the sake of the argument, assume that mutant cells originate in the ST-HSC compartment. In this case, they have an inherent disadvantage compared to the wild-type ST-HSCs, despite their larger self-renewal potential. The fitness of the wild-type cells in the ST-HSC compartment is determined by the combination of cell influx from the LT-HSCs (through differentiation) and the self-renewal of the wild-type ST-HSCs. In contrast, the fitness of the mutant ST-HSCs is determined only by their self-renewal rate (because no mutants are present among the upstream LT-HSCs). To overcome this inherent disadvantage of the mutant, the self-renewal potential of the mutant must be sufficiently large relative to that of the wild-type among the ST-HSCs for the mutant cells to invade there.

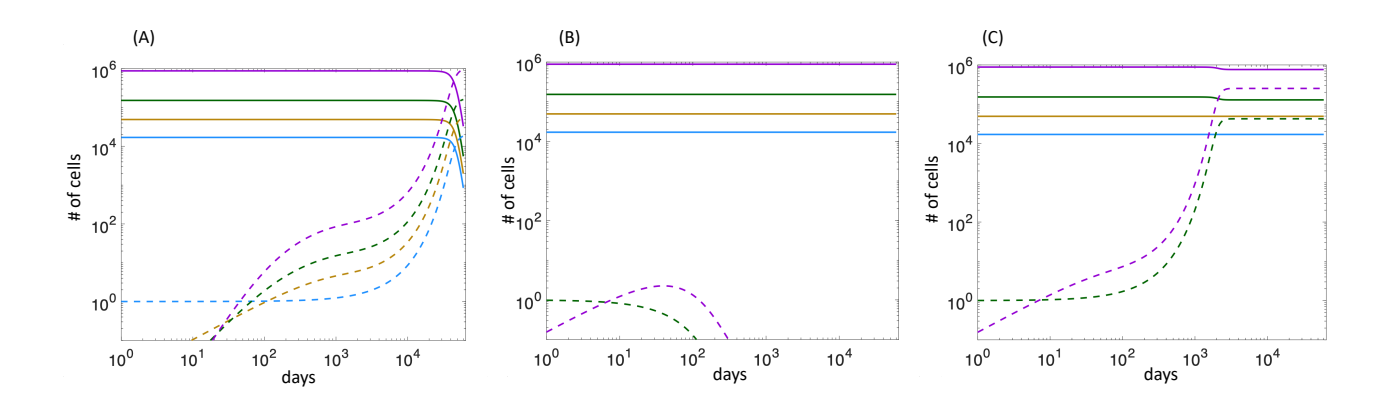


Figure 3: Simulated invasion dynamics of mutant cells. LT-HSCs, ST-HSCs, MPPs, and the sum of CMPs and CLPs are shown in blue, yellow, green, and purple lines, respectively. Solid line are wild-type cells, dashed line mutants. (A) A mutant with a 2% advantage is placed among LT-HSCs. (B) A mutant with a 2% advantage is placed among MPPs. Negative feedback on the self-renewal probabilities by cells in the same compartment was used, with h_0 =10⁻⁵, h_1 =10^{-5.5}, h_2 =10^{-5.5}. The rest of the parameters are given in Table1.

Figure 3 illustrates these concepts with computer simulations (see SI Section 3 for details of the mathematical analysis). The simulations start with the wild-type cell population at equilibrium (solid lines), and a small amount of advantageous mutant cells

(dashed lines) are introduced. First, a single mutant characterized by a 2% advantage is introduced among the LT-HSCs (Figure 3A). Over time, the mutants invade, although this takes a time frame longer than the life-span of a laboratory mouse (2.5 years) under the estimated parameters. Notably, although the mutant was introduced among LT-HSCs, it first rises among the downstream cells, because differentiation propagates the mutant into these compartments, where cell reproduction occurs with a faster rate. In Figure 3B, the same kind of mutant (2% advantage) is placed among the MPP cells. Due to the invasion barrier, however, the mutants fail to invade. In contrast, if a mutant with a very large advantage is placed among the MPPs (e.g. 25% advantage, Figure 3C), the invasion barrier is overcome and the mutant invades within a relatively short time span.

3.2 Evolutionary mechanisms to break the mutant invasion barrier in downstream compartments.

Let us consider mutant invasion in the ST-HSC cell population. According to the best fitting parameter estimate, a mutant would have to enjoy a >5.8% advantage to invade from low numbers. While possible for certain types of mutants, smaller fitness advantages (e.g. 2% or less) are more common. Here we explore mechanisms that could lead to the emergence of mutants with a relatively small fitness advantage.

According to our model, the mutant invasion barrier arises due to the influx of wild-type cells from upstream compartments through differentiation. A mutant that arises downstream, e.g. among ST-HSCs, lacks that influx, conferring an inherent disadvantage. Therefore, one way to reduce the mutant invasion barrier is to reduce the influx of wild-type cells from upstream compartments. This is what might occur during the aging process. Experimental data indicate that aging in mice results in a reduced rate at which HSCs divide and differentiate (8, 74, 75). In terms of our model, this can be expressed by an age (time)-dependent reduction of r_0x_0 . The model then predicts that an advantageous mutant arising among ST-HSCs or MPPs, which might not be

able to invade at a younger age, could successfully invade at an older age when the influx of upstream wild-type cells is diminished.

This is illustrated by computer simulations in Figure 4, using our base model where cells in each compartment exert negative feedback on their own self-renewal probabilities. A mutant with a 2% advantage is placed into the ST-HSC population at equilibrium. In a basic simulation, the mutant fails to grow due to the calculated invasion barrier (Figure 4A). In Figure 4B, the simulation is run such that the influx of wild-type cells from the LT-HSC compartment through differentiation (proportional to r_0x_0) is reduced by a small amount every time unit. Once the influx rate r_0x_0 falls below a

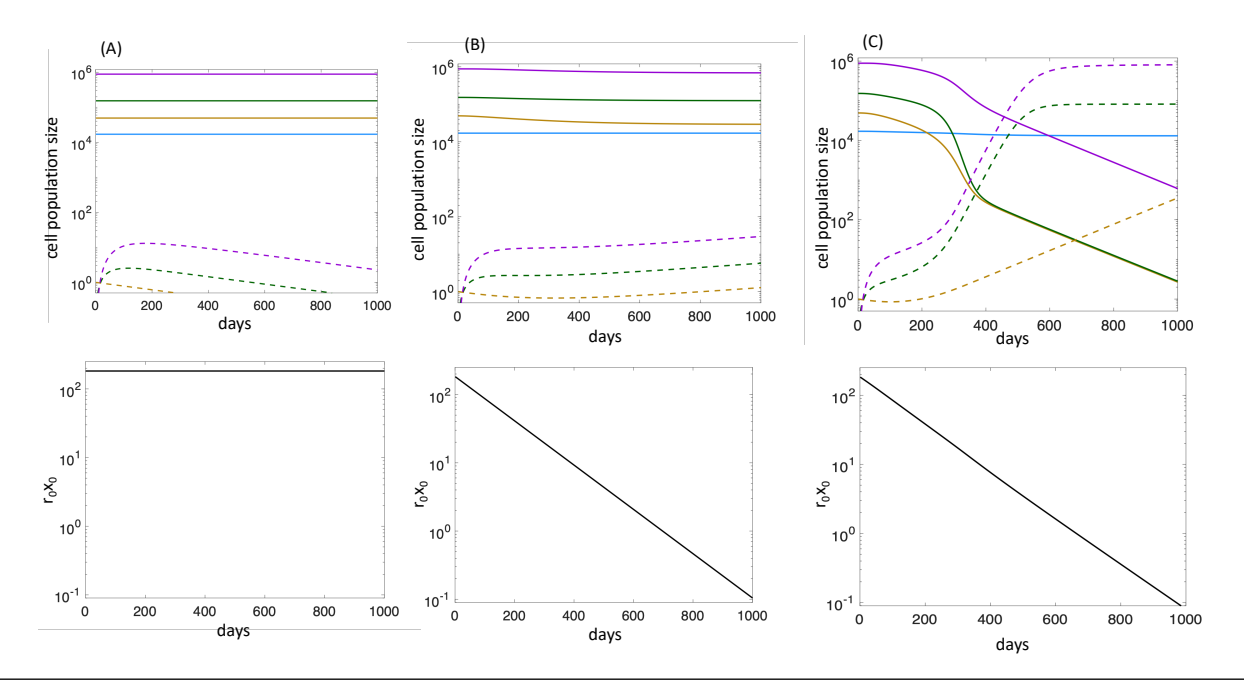


Figure 4. Computer simulations showing how mutants might overcome the invasion barrier in our model. A small amount of mutant cells is placed among ST-HSCs, while the wild-type cells are at equilibrium. In the top graphs, the dynamics of cell populations are shown, where LT-HSCs, ST-HSCs, MPPs, and the sum of CMPs and CLPs are shown in blue, yellow, green, and purple lines. Wild-type cells are shown by solid lines, mutant cells by dashed lines. The bottom graphs show the influx rate of LT-HSCs to ST-HSCs through differentiation (r₀x₀) over time. (A) model simulation without added mechanisms. The mutants fail to invade due to the barrier. (B) Aging-induced reduction of the rate of wild-type influx from LT-HSCs to ST-HSCs is modeled, by reducing the value of r_0x_0 by a factor of 1.0075 every day. Once the value of r_0x_0 has been sufficiently reduced, the mutant can invade, albeit slowly. (C) In addition to the reduction of r_0x_0 , we also assume that the most differentiated mutant cells in our model, $y_3^{(1)}+y_3^{(2)}$, induce inflammation, which reduces the self-renewal probability of wild-type cells in all compartments, but not of mutant cells. Hence, $p_0 = c_0/(h_0(x_0 + y_0) + \eta(y_{31} + y_{32}) + 1)$, $p_1 = c_1/(h_1(x_1 + y_1) + \eta(y_3^{(1)} + y_3^{(2)}) + 1)$, $p_2 = c_2/(h_2(x_2 + y_2)) + \eta(y_3^{(1)} + y_3^{(2)}) + 1$ $v_3^{(2)}$)+1), where η denotes rate at which wild-type cells are inhibited by mutant-induced inflammation. Now, mutant cells can emerge on a relatively fast time scale. We assumed that η =0.01. Negative feedback on the self-renewal probabilities by cells in the same compartment was used, with $h_0=10^{-5}$, $h_1=10^{-5.5}$, $h_2=10^{-5.5}$. The rest of the parameters are given in Table1.

threshold, the mutant cells start to grow from low numbers, meaning that the invasion barrier has been sufficiently reduced. At the same time, however, the mutant grows slowly and does not reach significant levels within the life-span of a laboratory mouse (about 2.5 years) in this parameter regime.

Another mechanism that might contribute to overcoming the mutant invasion barrier is based on the observation that certain mutants in the hematopoietic system (such as TET2 or DNMT3A mutants) are associated with an increased inflammatory environment, which has been investigated both mathematically and experimentally (76-79). Data indicate that inflammation might negatively influence the self-renewal capacity of wild-type cells, while affecting mutant cells to a lesser extent or not at all (80, 81). Indeed, it is thought that differentiated mutant cells themselves can induce increased inflammation (82, 83), thus turning conditions in favor of the mutant lineage (evolutionary niche construction). We incorporated this into our mathematical model by assuming that the self-renewal probability of wild-type (but not mutant) LT-HSCs, ST-HSCs, and MPPs is reduced proportionally to the number of mutant cells in the most differentiated compartments in our model (see Figure 4 for details of the formulation). We simultaneously assumed that the influx of wild-type cells from LT-HSCs to ST-HSCs is reduced due to aging, as described above. In this simulation, the reduction of wild-type influx from LT-HSCs to ST-HSCs eventually allows the mutant cell population to grow. First, this growth is slow as before (Figure 4C). Over time, however, mutant cell growth accelerates due to a positive feedback effect. An increase in the mutant population leads to increased inflammation levels, which in turn raises the relative fitness of mutants, and hence accelerates their growth. Through a combination of the reduced wild-type cell differentiation from LT-HSCs to ST-HSCs and mutant-induced inflammation, we can observe a significant rise in mutant abundance during the lifespan of a laboratory mouse (Figure 4C). Note that although the mutant was placed among the ST-HSCs, mutant invasion is predicted to be visible first in the downstream cell populations, due to their higher reproduction rates.

If the extent of mutant-induced inflammation is very strong, such that one mutant cell can already significantly increase the amount of inflammation, then the reduction of wild-type cell influx from LT-HSCs to ST-HSCs might not be needed to observe successful mutant growth. This, however, is probably not biologically realistic, because a certain amount of mutant growth is likely needed for them to sufficiently amplify inflammation levels. A generally high background level of chronic inflammation (e.g. due to an underlying disease or condition), however, might enable successful mutant invasion in the absence of an age-related reduction in wild-type cell influx from LT-HSCs to ST-HSCs.

We point out that longer-term sustained mutant presence might further require an increase in the cells' replicative capacity. As shown in SI Section 4, mutant invasion can be temporary if a mutant cell arising downstream (e.g. among ST-HSCs or MPPs) has limited replication capacity. In this case, further mutations might be needed to extend the replication capacity of mutant cells, thus enabling their long-term persistence. There is evidence that *tet2* and *dnmt3a* mutants already have an extended replicative capacity in mice (84, 85), meaning that with these mutants, no further increase in the cellular replication capacity might be needed for long-term mutant success.

4. Discussion and Conclusion

Quantitative data about the kinetics of cell division, self-renewal, and differentiation in LT-HSCs, ST-HSCs, and MPPs in mice (e.g. arising from label propagation experiments (7)) represent an invaluable source for the parameterization of mathematical models that describe hematopoiesis. Our analysis, however, has shown that the interpretation of these estimated parameters can change drastically if the mathematical models include non-linear homeostatic feedback control mechanisms. Without explicitly implementing homeostatic control mechanisms in mathematical models, the parameter estimates appear to suggest that while the LT-HSC population can maintain itself because self-renewal and differentiation processes are exactly balanced at homeostasis, this is not the case for ST-HSCs or MPPs: among those cells, differentiating divisions occur more frequently than self-renewal divisions at equilibrium,

implying that in the absence of LT-HSCs, these downstream populations will wash out. If feedback control is assumed to operate in the ST-HSC and MPP compartments, however, the dominance of differentiation divisions is compatible with the ability of these downstream cells to maintain themselves during homeostasis, even in the absence of LT-HSCs. The reason is that in the model, the dominance of differentiation divisions is the consequence of increased negative feedback on self-renewal that results from the influx of upstream cells (e.g. LT-HSC) through differentiation. If the upstream cells are removed, this feedback will be weaker, leading to an exact balance between self-renewal and differentiation events, as long as replication capacities are not exhausted. The model can thus reconcile the observation that transplanted ST-HSCs and MPPs (in the absence of upstream cells) can reconstitute a partial hematopoietic system and maintain it at homeostasis, before these cells reach their replication capacity (70-72). Similarly, following HSC and progenitor ablation in mice, HSC did not recover beyond 10% of normal numbers, while the progenitor cell population rebounded quickly and steady state hematopoiesis was for the most part not disrupted (73).

The model further suggests that feedback regulation in the ST-HSC and MPP compartments has important implications for the potential of advantageous mutants to emerge there. These compartments are thought to be important for mutant evolution because the cells replicate more frequently than LT-HSCs. Hence, chances to generate mutants are higher among ST-HSCs and MPPs compared to LT-HSCs. Due to the influx of wild-type cells from upstream compartments, however, competition among ST-HSCs and MPPs is more challenging for mutants. If a mutant is generated in one of those populations, the mutant competes with wild-type cells on two levels: (i) Through cell replication / loss dynamics within the compartment. If the mutant has a higher self-renewal rate than the wild-type, it will be advantageous in this respect. (ii) Through cell influx from the upstream compartments through differentiation. The mutant will be disadvantageous in this respect if it arose among the ST-HSCs or MPPs, because WT cells experience an influx from upstream compartments, while this is not the case for mutants (since they were only generated downstream). Therefore, to be able to spread in this setting, the replicative advantage of the mutants must be high enough to

overcome this mutant disadvantage. We have derived a simple formula for the mutant invasion threshold, in which the selection coefficient, s, of mutants must be higher than 1/(2p)-1, where p is the equilibrium self-renewal probability of the WT cells in the mutant's compartment of origin.

In contrast, mutants that arise among the LT-HSCs can grow to dominance in this model if they have any degree of advantage compared to the wild-type cells, no matter how small (note that setting p=1/2 in the formula above gives a zero threshold). The reason is that there are no upstream compartments, and hence no influx of wild-type cells. However, LT-HSCs are less likely to produce mutants due to infrequent cell divisions. Therefore, the model suggests that there is a tradeoff: It is unlikely for mutants to be created among LT-HSCs, but if they do emerge they can invade if they are advantageous. In contrast, it is more likely for mutants to be generated downstream, but the extent of the fitness advantage must lie above a threshold for them to be able to take-off.

With respect to the mutant invasion threshold calculated for the best fitting parameters (Table 1), it is important to keep in mind the confidence intervals. In particular, the estimate for the self-renewal probability of MPPs is characterized by relatively large confidence intervals, meaning that there is a degree of uncertainty regarding the exact magnitude of this invasion threshold (which was estimated to be around 20% from the best-fitting parameters). Hence, it is possible that this invasion threshold might be lower, and therefore more likely to be overcome by mutated cells. Even if a mutated cell does overcome the invasion threshold, however, our simulations indicate that mutant invasion would occur on a rather slow time scale relative to the lifespan of the organism. According to the parameterized model, robust mutant invasion within a biologically meaningful time frame would require the mutant advantage to be significantly larger than the invasion threshold (even for mutants emerging among MPPs), again pointing towards a strong barrier against mutant invasion.

This analysis suggests the existence of a strong resilience against mutant evolution in the hematopoietic system under biologically realistic parameters, and indicates that more complex conditions need to be present for mutant cell clones to grow. This has implications for the emergence of mutants that give rise to clonal hematopoiesis of indeterminate potential (CHIP), such as *TET2* and *DNMT3A* mutants. These mutants evolve in the hematopoietic system at homeostasis and increase the chances that hematological malignancies as well as other chronic health conditions develop (20). For these and other mutants in the hematopoietic system, inflammation has been identified as a possible selective force that drives their emergence (79-81), and this has also been formulated in previous mathematical models (76-79). Beyond this, it has been suggested that the mutants themselves induce an inflammatory environment (82, 83), which negatively affects wild-type cells but to a lesser extent mutant cells (80, 81), thus creating an increasingly advantageous environment for mutants (evolutionary niche construction). We investigated the effect of mutant-induced inflammation on the ability of mutant cells to overcome the invasion barrier in the model. The model suggested that mutant-induced inflammation on its own is unlikely to be sufficient to overcome the invasion barrier, because the mutant cell population first has to increase to a certain extent to induce sufficient inflammation. However, if additionally, aging results in a reduced influx of wild-type stem cells into downstream cell populations through differentiation (as has been shown experimentally (20)), the model suggests that this can reduce the invasion barrier to allow an initially slow mutant growth, which can then accelerate due to rising levels of mutant-induced inflammation (evolutionary niche construction). This suggests that complex dynamics are involved in the evolution of mutant cell clones in the hematopoietic system, and provides a guide for experimental testing. A better understanding of these complex dynamics will open doors for the design of evolution-based treatment interventions that can potentially reduce mutant burden and hence alleviate chronic health conditions and reduce the incidence of malignancies.

Our analysis of evolutionary dynamics occurred under the assumption that hematopoietic cell lineages are regulated by feedback control mechanisms during homeostasis, in particular feedback on the self-renewal rate of cells. It is instructive to compare these evolutionary dynamics to those occurring in the absence of feedback control, a setting in which mathematical models parameterized by experimental kinetic data have been analyzed in the past (66). Without feedback, only carcinogenic mutants can emerge, i.e. cell clones that grow uncontrolled, with a self-renewal rate that is larger than the differentiation rate. Because the self-renewal rate of LT-HSCs is exactly balanced by the differentiation rate, any degree of fitness advantage will result in uncontrolled mutant expansion without negative feedback. Because downstream cell populations (ST-HSCs and MPPs) differentiate more than they self-renew, models without feedback are also characterized by a mutant invasion threshold, although this is simply due to the fact that uncontrolled growth requires the self-renewal rate to exceed the rate of differentiation, which is more difficult to achieve in downstream compartments. The emergence of non-carcinogenic mutants (such as TET2 or DNMT3A mutants in CHIP) is not possible in models without feedback, and the invasion threshold for carcinogenic mutants is then not connected to the influx of wild-type cells from upstream compartments. In contrast, the presence of significant negative feedback in our model ensures that the population remains around a homeostatic steady state as evolution proceeds, and hence non-malignant mutants can emerge, competing with the wild-type cells through the shared feedback inhibition. The mutant invasion barrier for ST-HSCs and MPPs described here arises in our models with feedback due to a different mechanism compared to models without feedback (66). The invasion threshold in our models with feedback control is connected to competition dynamics, and occurs because the influx of wild-type cells from upstream compartments (and a corresponding lack of influx of mutant cells) confers an inherent disadvantage to the mutant cells, even though they have a higher reproductive fitness in the compartment in which they arise (ST-HSCs or MPPs).

In our model with feedback, the development of uncontrolled cell growth would require further mutations that allow cells to escape feedback-mediated homeostasis (69). If the degree of negative feedback is significantly weakened (but not absent) in our model, however, the equilibrium level to which invading advantageous mutants grow in

the system becomes higher (see SI Appendix Section 3, Figures S7 and S9), which could represent an intermediate stage in the loss of homeostasis.

While the model structure used in this study is based on the previous literature on modeling the hematopoietic system (21-25) and other tissues (86, 87), there are uncertainties regarding the exact processes that should be included in such models for maximal biological realism. All cell divisions in our model are symmetric, and the balance between self-renewal (e.g. a stem cell giving rise to two stem cells) and differentiation (e.g. a stem cell giving rise to two differentiated cells) is determined on the population level. For example, at homeostasis, half of all LT-HSC divisions are selfrenewing symmetric divisions, and half are differentiating symmetric divisions. Even though there is empirical evidence for this mechanism in mammalian tissues (88, 89), it is possible that asymmetric cell divisions also take place in the hematopoietic system (90), e.g. a stem cell giving rise to one daughter stem cell and one daughter differentiated cell. When asymmetric stem cell divisions are added to the type of models analyzed here, many properties remain the same (91), and we do not expect conclusions to change if asymmetric cell divisions occur among the LT-HSCs. With downstream cells, asymmetric cell divisions are unlikely to play a significant role because at homeostasis, self-renewal and differentiating divisions are not balanced.

A related issue is the mechanism underlying differentiation processes. In our model, differentiation is coupled to cell division. There is experimental evidence that HSC fate decisions are connected to the cell cycle, e.g. through changes in metabolism (92, 93), thus supporting our model assumptions. On the other hand, the differentiation of LT-HSCs has been shown to occur in the absence of cell division in certain circumstances (94), although it is not clear how frequently division-independent differentiation events occur. More complex assumptions about differentiation mechanisms can be incorporated into models as more biological information becomes available in the future. Another source of uncertainty concerns the mechanisms that contribute to homeostasis. We modeled feedback in a general way, analyzing a multitude of ways in which feedback control can contribute to homeostasis. Biologically, this can account for both signals that are secreted from the cell lineage itself, and from

the microenvironment that senses the abundance of various cell linage sub-populations. Other aspects that might limit the number of cells at homeostasis and that are not part of our model could be spatial constraints (95), as well as interactions with the extracellular matrix (96). Incorporating these into the current model is a more complex effort and beyond the scope of our study.

The insights obtained from our model can suggest new mouse transplant experiments to test some of these notions, where mutant and wild-type cells tagged with different luciferases are transplanted together, and the relative fraction of mutants is monitored non-invasively over the long-term. Mutant cells can be purified to only include mutant ST-HSCs or MPPs (based on markers), and the fate of the mutants in the different compartment can be tracked. Due to the invasion barriers, we expect the relative fraction of the mutants to decline over time. This experiment could be repeated in the presence of various degrees inflammation, for example induced by LPS. Based on our model, we hypothesize that sufficient inflammation levels help mutants overcome the invasion barrier. This set of experiments could then be repeated, where mutants are present in all cell compartments, including LT-HSCs. Based on our model analysis, we hypothesize that in this case, the mutant fraction will not decline over time even without any inflammation, due to both wild-type and mutant cells being present among the LT-HSCs.

5. Materials and methods

The mathematical model used in this work is based on ordinary differential equations, where we keep track of cell dynamics in the 5 compartments: LT-HSCs, SH-HSCs, MPPs, CMPs, and CLPs, and include the processes of cell self-renewal, cell differentiation (assumed to be associated with cell divisions), and cell removal from the CMP and CLP compartments. The details are presented in SI Appendix. The model is calibrated by using previously published experimental data (SI Section 1). The probabilities of self-renewal in the LT-HSC, SH-HSC, and MPP compartments are assumed to be functions of cell populations in different compartments. In order to study evolutionary dynamics, we incorporate mutant cells in the system of ODEs and consider

the stability of a mutant-free equilibrium. We assume that advantageous mutants can be characterized by (i) an increased rate of cell divisions and (ii) an increased probability of self-renewal, SI Section 2. We then proceed to show that differences of type (i) cannot result in mutants growing from low numbers. On the other hand, type (ii) differences can lead to a positive selection of mutants. While a standard stability analysis yields that mutants with any degree of type (ii) advantage will destabilize the equilibrium, a more detailed set of calculations shows that mutants that originate in SH-HSC or MPP compartments have to overcome an invasion barrier. SI Section 2 demonstrates this result, which is independent of specific assumptions about the shape of control functions. Several scenarios of mutant dynamics are studied in SI Section 3, including an example of stochastic modeling. Replication limits are included in the model in Section 4, when we also consider a third type of mutants, characterized by (iii) an increased replication limit. It is shown that in the presence of replication limits, the invasion threshold result still holds, but now type (iii) differences are required for the mutants to make a longer lasting impact on system dynamics.

References

- 1. E. M. Pietras *et al.*, Functionally distinct subsets of lineage-biased multipotent progenitors control blood production in normal and regenerative conditions. *Cell stem cell* **17**, 35-46 (2015).
- 2. D. Bryder, D. J. Rossi, I. L. Weissman, Hematopoietic stem cells: the paradigmatic tissue-specific stem cell. *The American journal of pathology* **169**, 338-346 (2006).
- 3. I. L. Weissman, J. A. Shizuru, The origins of the identification and isolation of hematopoietic stem cells, and their capability to induce donor-specific transplantation tolerance and treat autoimmune diseases. *Blood, The Journal of the American Society of Hematology* **112**, 3543-3553 (2008).
- 4. J. Domen, I. L. Weissman, Self-renewal, differentiation or death: regulation and manipulation of hematopoietic stem cell fate. *Molecular medicine today* **5**, 201-208 (1999).
- 5. J. Seita, I. L. Weissman, Hematopoietic stem cell: self-renewal versus differentiation. *Wiley Interdisciplinary Reviews: Systems Biology and Medicine* **2**, 640-653 (2010).
- 6. A. C. Wilkinson, K. J. Igarashi, H. Nakauchi, Haematopoietic stem cell self-renewal in vivo and ex vivo. *Nature Reviews Genetics* **21**, 541-554 (2020).
- 7. K. Busch *et al.*, Fundamental properties of unperturbed haematopoiesis from stem cells in vivo. *Nature* **518**, 542-546 (2015).

- 8. P. Säwen *et al.*, Murine HSCs contribute actively to native hematopoiesis but with reduced differentiation capacity upon aging. *Elife* **7**, e41258 (2018).
- 9. S. Kim *et al.*, Dynamics of HSPC repopulation in nonhuman primates revealed by a decade-long clonal-tracking study. *Cell stem cell* **14**, 473-485 (2014).
- 10. J. Sun et al., Clonal dynamics of native haematopoiesis. Nature **514**, 322-327 (2014).
- 11. Y. Pan, M. R. D'Orsogna, M. Tang, T. Stiehl, T. Chou, Clonal abundance patterns in hematopoiesis: Mathematical modeling and parameter estimation. *Frontiers in Systems Biology* **3**, 893366 (2023).
- 12. S. Goyal, S. Kim, I. S. Chen, T. Chou, Mechanisms of blood homeostasis: lineage tracking and a neutral model of cell populations in rhesus macaques. *BMC biology* **13**, 1-14 (2015).
- 13. S. Upadhaya *et al.*, Kinetics of adult hematopoietic stem cell differentiation in vivo. *Journal of Experimental Medicine* **215**, 2815-2832 (2018).
- 14. S. Xu, S. Kim, I. S. Chen, T. Chou, Modeling large fluctuations of thousands of clones during hematopoiesis: The role of stem cell self-renewal and bursty progenitor dynamics in rhesus macaque. *PLoS computational biology* **14**, e1006489 (2018).
- 15. B. A. Anthony, D. C. Link, Regulation of hematopoietic stem cells by bone marrow stromal cells. *Trends in immunology* **35**, 32-37 (2014).
- 16. B. Göttgens, Regulatory network control of blood stem cells. *Blood, The Journal of the American Society of Hematology* **125**, 2614-2620 (2015).
- 17. D. Link, M. Walter, 'CHIP'ping away at clonal hematopoiesis. *Leukemia* **30**, 1633-1635 (2016).
- 18. N. A. Robertson *et al.*, Longitudinal dynamics of clonal hematopoiesis identifies genespecific fitness effects. *Nature medicine* **28**, 1439-1446 (2022).
- 19. M. A. Fabre *et al.*, The longitudinal dynamics and natural history of clonal haematopoiesis. *Nature* **606**, 335-342 (2022).
- 20. S. Jaiswal, B. L. Ebert, Clonal hematopoiesis in human aging and disease. *Science* **366**, eaan4673 (2019).
- 21. T. Stiehl, A. Marciniak-Czochra, Stem cell self-renewal in regeneration and cancer: insights from mathematical modeling. *Current opinion in systems biology* **5**, 112-120 (2017).
- 22. T. Lorenzi, A. Marciniak-Czochra, T. Stiehl, A structured population model of clonal selection in acute leukemias with multiple maturation stages. *J Math Biol* **79**, 1587-1621 (2019).
- 23. S. Chulián *et al.*, Dynamical properties of feedback signalling in B lymphopoiesis: A mathematical modelling approach. *Journal of theoretical biology* **522**, 110685 (2021).
- 24. R. K. Pedersen, M. Andersen, T. Stiehl, J. T. Ottesen, Mathematical modelling of the hematopoietic stem cell-niche system: Clonal dominance based on stem cell fitness. *Journal of theoretical biology* **518**, 110620 (2021).
- 25. M. Brunetti, M. C. Mackey, M. Craig, Understanding normal and pathological hematopoietic stem cell biology using mathematical modelling. *Current Stem Cell Reports* **7**, 109-120 (2021).
- 26. A. L. MacLean, S. Filippi, M. P. Stumpf, The ecology in the hematopoietic stem cell niche determines the clinical outcome in chronic myeloid leukemia. *Proceedings of the National Academy of Sciences* **111**, 3883-3888 (2014).
- 27. D. Dingli, A. Traulsen, J. M. Pacheco, Compartmental architecture and dynamics of hematopoiesis. *PloS one* **2**, e345 (2007).
- 28. T. Stiehl, W. Wang, C. Lutz, A. Marciniak-Czochra, Mathematical modeling provides evidence for niche competition in human AML and serves as a tool to improve risk stratification. *Cancer research* **80**, 3983-3992 (2020).

- 29. A. L. MacLean, C. Lo Celso, M. P. Stumpf, Population dynamics of normal and leukaemia stem cells in the haematopoietic stem cell niche show distinct regimes where leukaemia will be controlled. *Journal of the Royal Society Interface* **10**, 20120968 (2013).
- 30. T. Székely Jr, K. Burrage, M. Mangel, M. B. Bonsall, Stochastic dynamics of interacting haematopoietic stem cell niche lineages. *PLoS computational biology* **10**, e1003794 (2014).
- 31. M. Mangel, M. B. Bonsall, Phenotypic evolutionary models in stem cell biology: replacement, quiescence, and variability. *PloS one* **3**, e1591 (2008).
- 32. I. Roeder, M. Loeffler, A novel dynamic model of hematopoietic stem cell organization based on the concept of within-tissue plasticity. *Experimental hematology* **30**, 853-861 (2002).
- 33. B. Werner, D. Dingli, A. Traulsen, A deterministic model for the occurrence and dynamics of multiple mutations in hierarchically organized tissues. *Journal of The Royal Society Interface* **10**, 20130349 (2013).
- 34. T. Stiehl, A. Marciniak-Czochra, Characterization of stem cells using mathematical models of multistage cell lineages. *Mathematical and Computer Modelling* **53**, 1505-1517 (2011).
- 35. Y. Nakata, P. Getto, A. Marciniak-Czochra, T. Alarcón, Stability analysis of multi-compartment models for cell production systems. *Journal of biological dynamics* **6**, 2-18 (2012).
- 36. T. Stiehl, N. Baran, A. D. Ho, A. Marciniak-Czochra, Clonal selection and therapy resistance in acute leukaemias: mathematical modelling explains different proliferation patterns at diagnosis and relapse. *Journal of The Royal Society Interface* **11**, 20140079 (2014).
- 37. T. Stiehl, A. Marciniak-Czochra, Mathematical modeling of leukemogenesis and cancer stem cell dynamics. *Mathematical Modelling of Natural Phenomena* **7**, 166-202 (2012).
- 38. H.-E. Wichmann, M. Loeffler, *Mathematical modeling of cell proliferation: stem cell regulation in hemopoiesis* (CRC Pr I Llc, 1985).
- 39. S. Schmitz, H. Franke, J. Brusis, H. Wichmann, Quantification of the cell kinetic effects of G-CSF using a model of human granulopoiesis. *Experimental hematology* **21**, 755-760 (1993).
- 40. M. C. Mackey, Cell kinetic status of haematopoietic stem cells. *Cell proliferation* **34**, 71-83 (2001).
- 41. M. C. Mackey, Mathematical models of hematopoietic cell replication and control. *Case Studies in Mathematical Modeling–Ecology, Physiology and Cell Biology. New Jersey, Prentice-Hall*, 151-182 (1997).
- 42. J. M. Mahaffy, J. Bélair, M. C. Mackey, Hematopoietic model with moving boundary condition and state dependent delay: applications in erythropoiesis. *Journal of theoretical biology* **190**, 135-146 (1998).
- 43. M. C. Mackey, J. G. Milton, Feedback, delays and the origin of blood cell dynamics. (1990).
- 44. I. Roeder, R. Lorenz, Asymmetry of stem cell fate and the potential impact of the niche: observations, simulations, and interpretations. *Stem Cell Rev* **2**, 171-180 (2006).
- 45. I. Roederer et al., Leukemia stem cells hit or miss. Nature medicine Fill in (2006).
- 46. C. Marquet, M. Adimy, On the stability of hematopoietic model with feedback control. *Comptes Rendus. Mathématique* **350**, 173-176 (2012).
- 47. L. Pujo-Menjouet, S. Bernard, M. C. Mackey, Long period oscillations in a G 0 model of hematopoietic stem cells. *SIAM Journal on Applied Dynamical Systems* **4**, 312-332 (2005).

- 48. T. Cassidy, A. R. Humphries, M. Craig, M. C. Mackey, Characterizing chemotherapy-induced neutropenia and monocytopenia through mathematical modelling. *Bulletin of mathematical biology* **82**, 1-26 (2020).
- 49. D. C. De Souza, A. R. Humphries, Dynamics of a mathematical hematopoietic stem-cell population model. *SIAM Journal on Applied Dynamical Systems* **18**, 808-852 (2019).
- 50. T. Stiehl, A. Ho, A. Marciniak-Czochra, The impact of CD34+ cell dose on engraftment after SCTs: personalized estimates based on mathematical modeling. *Bone marrow transplantation* **49**, 30-37 (2014).
- 51. R. Kumar, S. R. Shah, T. Stiehl, Understanding the impact of feedback regulations on blood cell production and leukemia dynamics using model analysis and simulation of clinically relevant scenarios. *Applied Mathematical Modelling* (2024).
- 52. A. Marciniak-Czochra, T. Stiehl, A. D. Ho, W. Jäger, W. Wagner, Modeling of asymmetric cell division in hematopoietic stem cells—regulation of self-renewal is essential for efficient repopulation. *Stem cells and development* **18**, 377-386 (2009).
- 53. A. Marciniak-Czochra, T. Stiehl, W. Wagner, Modeling of replicative senescence in hematopoietic development. *Aging (Albany NY)* **1**, 723 (2009).
- 54. T. Stiehl, N. Baran, A. D. Ho, A. Marciniak-Czochra, Cell division patterns in acute myeloid leukemia stem-like cells determine clinical course: a model to predict patient survival. *Cancer research* **75**, 940-949 (2015).
- 55. T. Walenda *et al.*, Feedback signals in myelodysplastic syndromes: increased self-renewal of the malignant clone suppresses normal hematopoiesis. *PLoS computational biology* **10**, e1003599 (2014).
- 56. Y. Kheifetz, M. Scholz, Modeling individual time courses of thrombopoiesis during multicyclic chemotherapy. *PLoS computational biology* **15**, e1006775 (2019).
- 57. L. E. Friberg, A. Henningsson, H. Maas, L. Nguyen, M. O. Karlsson, Model of chemotherapy-induced myelosuppression with parameter consistency across drugs. *Journal of clinical oncology* **20**, 4713-4721 (2002).
- 58. M. Scholz, A. Gross, M. Loeffler, A biomathematical model of human thrombopoiesis under chemotherapy. *Journal of theoretical biology* **264**, 287-300 (2010).
- 59. L. E. Friberg, M. O. Karlsson, Mechanistic models for myelosuppression. *Investigational new drugs* **21**, 183-194 (2003).
- 60. M. Scholz, C. Engel, M. Loeffler, Modelling human granulopoiesis under polychemotherapy with G-CSF support. *J Math Biol* **50**, 397-439 (2005).
- 61. C. Colijn, M. C. Mackey, A mathematical model of hematopoiesis—I. Periodic chronic myelogenous leukemia. *Journal of theoretical biology* **237**, 117-132 (2005).
- 62. C. Colijn, M. C. Mackey, A mathematical model of hematopoiesis: II. Cyclical neutropenia. *Journal of theoretical biology* **237**, 133-146 (2005).
- 63. R. Apostu, M. C. Mackey, Understanding cyclical thrombocytopenia: A mathematical modeling approach. *Journal of theoretical biology* **251**, 297-316 (2008).
- 64. Z. L. Whichard, C. A. Sarkar, M. Kimmel, S. J. Corey, Hematopoiesis and its disorders: a systems biology approach. *Blood, The Journal of the American Society of Hematology* **115**, 2339-2347 (2010).
- 65. G. Clapp, D. Levy, A review of mathematical models for leukemia and lymphoma. *Drug Discovery Today: Disease Models* **16**, 1-6 (2015).
- 66. M. Takahashi *et al.*, Reconciling flux experiments for quantitative modeling of normal and malignant hematopoietic stem/progenitor dynamics. *Stem cell reports* **16**, 741-753 (2021).
- 67. M. Klose, M. C. Florian, A. Gerbaulet, H. Geiger, I. Glauche, Hematopoietic stem cell dynamics are regulated by progenitor demand: lessons from a quantitative modeling approach. *Stem cells* **37**, 948-957 (2019).

- 68. M. Barile *et al.*, Hematopoietic stem cells self-renew symmetrically or gradually proceed to differentiation. *BioRxiv*, 2020.2008. 2006.239186 (2020).
- 69. I. A. Rodriguez-Brenes, N. L. Komarova, D. Wodarz, Evolutionary dynamics of feedback escape and the development of stem-cell-driven cancers. *Proceedings of the National Academy of Sciences of the United States of America* **108**, 18983-18988 (2011).
- 70. D. Bhattacharya, D. Bryder, D. J. Rossi, I. L. Weissman, Rapid lymphocyte reconstitution of unconditioned immunodeficient mice with non-self-renewing multipotent hematopoietic progenitors. *Cell cycle* **5**, 1135-1139 (2006).
- 71. R. Yamamoto *et al.*, Clonal analysis unveils self-renewing lineage-restricted progenitors generated directly from hematopoietic stem cells. *Cell* **154**, 1112-1126 (2013).
- 72. J. Carrelha *et al.*, Hierarchically related lineage-restricted fates of multipotent haematopoietic stem cells. *Nature* **554**, 106-111 (2018).
- 73. K. B. Schoedel *et al.*, The bulk of the hematopoietic stem cell population is dispensable for murine steady-state and stress hematopoiesis. *Blood, The Journal of the American Society of Hematology* **128**, 2285-2296 (2016).
- 74. M. S. Kowalczyk *et al.*, Single-cell RNA-seq reveals changes in cell cycle and differentiation programs upon aging of hematopoietic stem cells. *Genome research* **25**, 1860-1872 (2015).
- 75. S. Noda, H. Ichikawa, H. Miyoshi, Hematopoietic stem cell aging is associated with functional decline and delayed cell cycle progression. *Biochemical and biophysical research communications* **383**, 210-215 (2009).
- 76. M. Andersen *et al.*, Mathematical modelling as a proof of concept for MPNs as a human inflammation model for cancer development. *PloS one* **12**, e0183620 (2017).
- 77. J. T. Ottesen, M. Andersen, Aging, Inflammation, and Comorbidity in Cancers—A General In Silico Study Exemplified by Myeloproliferative Malignancies. *Cancers* **15**, 4806 (2023).
- 78. J. T. Ottesen *et al.*, Bridging blood cancers and inflammation: The reduced Cancitis model. *Journal of theoretical biology* **465**, 90-108 (2019).
- 79. A. Heyde *et al.*, Increased stem cell proliferation in atherosclerosis accelerates clonal hematopoiesis. *Cell* **184**, 1348-1361. e1322 (2021).
- 80. S. O. Abegunde, R. Buckstein, R. A. Wells, M. J. Rauh, An inflammatory environment containing TNFα favors Tet2-mutant clonal hematopoiesis. *Experimental hematology* **59**, 60-65 (2018).
- 81. M. A. Florez *et al.*, Clonal hematopoiesis: Mutation-specific adaptation to environmental change. *Cell stem cell* **29**, 882-904 (2022).
- 82. J. J. Fuster *et al.*, Clonal hematopoiesis associated with TET2 deficiency accelerates atherosclerosis development in mice. *Science* **355**, 842-847 (2017).
- 83. S. Jaiswal *et al.*, Clonal hematopoiesis and risk of atherosclerotic cardiovascular disease. *New England Journal of Medicine* **377**, 111-121 (2017).
- 84. M. Jeong *et al.*, Loss of Dnmt3a immortalizes hematopoietic stem cells in vivo. *Cell reports* **23**, 1-10 (2018).
- 85. K. Moran-Crusio *et al.*, Tet2 loss leads to increased hematopoietic stem cell self-renewal and myeloid transformation. *Cancer cell* **20**, 11-24 (2011).
- 86. A. D. Lander, K. K. Gokoffski, F. Y. Wan, Q. Nie, A. L. Calof, Cell lineages and the logic of proliferative control. *PLoS biology* **7**, e15 (2009).
- 87. W. C. Lo *et al.*, Feedback regulation in multistage cell lineages. *Math Biosci Eng* **6**, 59-82 (2009).
- 88. H. J. Snippert *et al.*, Intestinal crypt homeostasis results from neutral competition between symmetrically dividing Lgr5 stem cells. *Cell* **143**, 134-144 (2010).
- 89. B. D. Simons, H. Clevers, Strategies for homeostatic stem cell self-renewal in adult tissues. *Cell* **145**, 851-862 (2011).

- 90. B. Giebel, I. Bruns, Self-renewal versus differentiation in hematopoietic stem and progenitor cells: a focus on asymmetric cell divisions. *Current stem cell research & therapy* **3**, 9-16 (2008).
- 91. L. D. Weiss, P. van den Driessche, J. S. Lowengrub, D. Wodarz, N. L. Komarova, Effect of feedback regulation on stem cell fractions in tissues and tumors: Understanding chemoresistance in cancer. *Journal of theoretical biology* **509**, 110499 (2021).
- 92. S. Treichel, M.-D. Filippi, Linking cell cycle to hematopoietic stem cell fate decisions. *Frontiers in Cell and Developmental Biology* **11**, 1231735 (2023).
- 93. K. Ito, K. Ito, Hematopoietic stem cell fate through metabolic control. *Experimental hematology* **64**, 1-11 (2018).
- 94. T. Grinenko *et al.*, Hematopoietic stem cells can differentiate into restricted myeloid progenitors before cell division in mice. *Nature communications* **9**, 1898 (2018).
- 95. P. Uhl, J. Lowengrub, N. Komarova, D. Wodarz, Spatial dynamics of feedback and feedforward regulation in cell lineages. *PLoS computational biology* **18**, e1010039 (2022).
- 96. S. Nallanthighal, J. P. Heiserman, D.-J. Cheon, The role of the extracellular matrix in cancer stemness. *Frontiers in cell and developmental biology* **7**, 86 (2019).

Dynamically adjusted cell fate decisions and resilience to mutant invasion during steady state hematopoiesis revealed by an experimentally parameterized mathematical model

Supplementary materials

Contents

1	Wil	d-type ODE models and their properties	2
	1.1	Model parameterization	2
	1.2	The self-renewal probability functions and model calibration .	5
2	Modeling wild-type and mutant co-dynamics		
	2.1	ODEs for wild type and mutant cells	9
	2.2	The mutant-free equilibrium and its stability	10
	2.3	Fitness thresholds for mutant invasion	14
3	3 The fate of mutants originating in different compartment		16
	3.1	Mutants originating in C_0 : pure mutant solutions	16
	3.2	Mutants originating in downstream compartments	18
	3.3	Control of "self" type, mutants originating in C_1 : a case study	21
	3.4	Threshold conditions and stochastic modeling	23
4	Incl	luding replication limits in the lineage dynamics	27
	4.1	The wild type system	27
	4.2	Co-dynamics of wild-type and mutant cells	29

1 Wild-type ODE models and their properties

Model parameterization 1.1

We describe hematopoietic turnover by the following system of ODEs:

$$\frac{dx_0}{dt} = r_0 x_0 (2p_0 - 1), (1)$$

$$\frac{dx_1}{dt} = 2r_0x_0(1-p_0) + r_1x_1(2p_1-1), \tag{2}$$

$$\frac{dx_2}{dt} = 2r_1x_1(1-p_1) + r_2x_2(2p_2-1), \tag{3}$$

$$\frac{dx_0}{dt} = r_0 x_0 (2p_0 - 1), \qquad (1)$$

$$\frac{dx_1}{dt} = 2r_0 x_0 (1 - p_0) + r_1 x_1 (2p_1 - 1), \qquad (2)$$

$$\frac{dx_2}{dt} = 2r_1 x_1 (1 - p_1) + r_2 x_2 (2p_2 - 1), \qquad (3)$$

$$\frac{dx_3^{(1)}}{dt} = 2r_2 x_2 (1 - p_2) \gamma^{(1)} - d_3^{(1)} x_3^{(1)}, \qquad (4)$$

$$\frac{dx_2^{(2)}}{dt} = 2r_2 x_2 (1 - p_2) \gamma^{(2)} - d_3^{(2)} x_3^{(2)}, \qquad (4)$$

$$\frac{dx_3^{(2)}}{dt} = 2r_2x_2(1-p_2)\gamma^{(2)} - d_3^{(2)}x_3^{(2)}, \tag{5}$$

where the variables $x_0(t), x_1(t)$ and $x_2(t)$ denote the populations of the LT-HSC, ST-HSC, and MPP compartments respectively, and variables $x_3^{(1)}$ and $x_3^{(2)}$ describe the CMP and CLP compartments. The corresponding schematic can be found in figure S1(a).

We assume that the probabilities of self-renewal, p_0, p_1 and p_2 are some functions of the cell populations:

$$p_i = p_i(x_0, x_1, x_2, x_3^{(1)}, x_3^{(2)}), \quad 0 \le i \le 2.$$

We will denote the equilibrium population sizes by capital letters. Solving equations (1,5) in steady state, we obtain:

$$X_1 = \frac{r_0 X_0}{r_1 (1 - 2\bar{p}_1)}, \tag{6}$$

$$X_2 = \frac{2r_0X_0(1-\bar{p}_1)}{r_2(1-2\bar{p}_1)(1-2\bar{p}_2)},\tag{7}$$

$$X_3^{(1)} = \frac{4r_0 X_0 (1 - \bar{p}_1)(1 - \bar{p}_2) \gamma^{(1)}}{d_3^{(1)} (1 - 2\bar{p}_1)(1 - 2\bar{p}_2)}, \tag{8}$$

$$X_3^{(2)} = \frac{4r_0X_0(1-\bar{p}_1)(1-\bar{p}_2)\gamma^{(2)}}{d_3^{(2)}(1-2\bar{p}_1)(1-2\bar{p}_2)}, \tag{9}$$

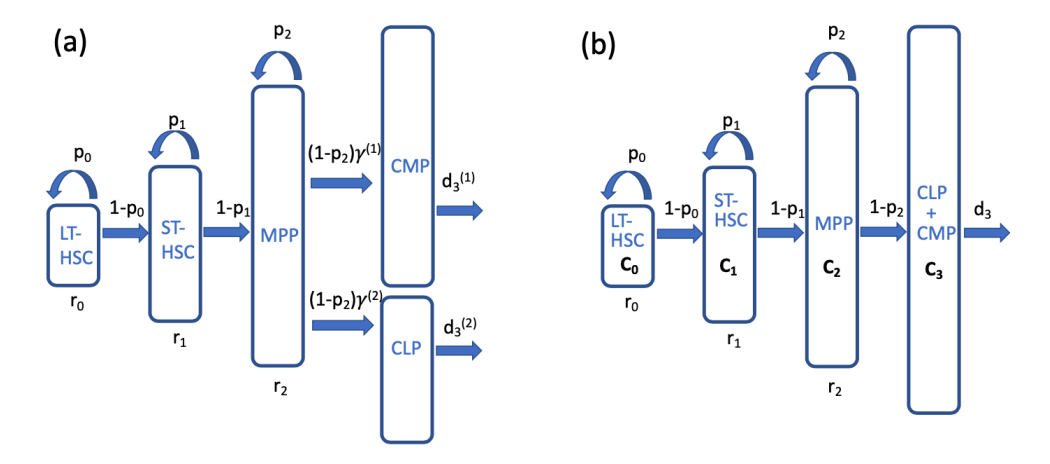


Figure S1: Schematic representations of the compartment system and the processes/rates included in the model. (a) The model with separate CMP and CLP compartments. (b) The model with compartments CMP and CLP combined into compartment C_3 .

where we denoted

$$\bar{p}_i = p_i(X_0, X_1, X_2, X_3^{(1)}, X_3^{(2)}), \quad 0 \le i \le 2,$$

the equilibrium values of the probabilities of self-renewal.

To determine numerical parameters of the model, we used the neutral label propagation data and the relative compartment size data, measured in \square and \square . Let us denote the numbers of cells marked with a neutral label as $z_i(t)$ in each of the compartments. The equations for z_i are in this case identical to equations \square , and the probabilities of self-renewal /differentiation are evaluated at the equilibrium (and are thus constants).

Denote by $f_i \equiv \frac{z_i}{X_i}$ the fraction of labeled population in each compartment. We have

$$\dot{f}_0 = 0, \tag{10}$$

$$\dot{f}_1 = \frac{1}{\tau_1}(f_0 - f_1),$$
 (11)

$$\dot{f}_2 = \frac{1}{\tau_2} (f_1 - f_2), \tag{12}$$

$$\dot{f}_3^{(1)} = \frac{\tau_2}{\tau_3^{(1)}} (f_2 - f_3^{(1)}), \quad \dot{f}_3^{(2)} = \frac{1}{\tau_3^{(2)}} (f_2 - f_3^{(2)}), \tag{13}$$

where

$$\tau_1 = \frac{1}{r_1(1 - 2\bar{p}_1)}, \quad \tau_2 = \frac{1}{r_2(1 - 2\bar{p}_2)}, \quad \tau_3^{(1)} = \frac{1}{d_3^{(1)}}, \quad \tau_3^{(2)} = \frac{1}{d_3^{(2)}}.$$
(14)

The ratios of the compartment sizes at the equilibrium satisfy:

$$\frac{X_1}{X_0} = \frac{r_0}{r_1(1 - 2\bar{p}_1)}, \quad \frac{X_2}{X_1} = \frac{2r_1(1 - \bar{p}_1)}{r_2(1 - 2\bar{p}_2)}, \quad \frac{X_3^{(1)}}{X_2} = \frac{2r_2\gamma_2^{(1)}}{d_3^{(1)}}, \quad \frac{X_3^{(2)}}{X_2} = \frac{2r_2\gamma_2^{(2)}}{d_3^{(2)}}.$$
(15)

Following the methodology described in $[\![\!]\!]$, we fitted the analytical solutions of equations $(\![\!]\!]$ 10, to the time-series of the neutral label proportions in compartments ST-HSC,MPP, CMP, and CLP (using proportions relative to that in the LT-HSC compartment); in addition, the relative compartment sizes were fitted. The prediction for the relative compartment sizes, $\nu_1 = X_1/X_0, \nu_2 = X_2/X_1, \nu_3^{(1)} = X_3^{(1)}/X_2$, and $\nu_3^{(2)} = X_3^{(2)}/X_2$ were obtained from solutions $(\![\![\![\![\![\![\!]\!]\!]\!]\!]\!]$, and fitted to the quantities reported in $[\![\![\![\!]\!]\!]\!]\!]$, which were determined by cell counting of cell suspensions. Note that despite differences in the equations for cell populations used here and in $[\![\![\![\!]\!]\!]\!]\!]$, are identical for our model. In the fitting procedure, we used a larger, updated dataset for the time-series in the ST-HSC and MPP compartments, see $[\![\![\![\!]\!]\!]\!]\!]\!]$.

In order to investigate confidence intervals of the fitted parameters, and also the confidence intervals of the fit, we used the bootstrapping method to resample the data, assuming the beta-distribution of the quantities f_1 , f_2 , $f_3^{(1)}$, and $f_3^{(2)}$ (the usual assumption of normality does not hold in the case where the variables are fractions). The two parameters of the beta-distribution were calculated from the mean and standard deviation information provided in the data. The best fits together with the confidence intervals are shown in figure $\S 2$. The results for the best-fitting parameters together with the confidence intervals are presented in Table 1 of the main text.

In what follows we will combine compartments CMP and CLP into a single compartment, which allows for a simpler model, see the schematic of figure S1b. To generalize the description, suppose that there are n+1 compartments, C_0, \ldots, C_n , that have increasing degree of differentiation (in our case n=3). Denote by x_i the number of wild type cells in compartment

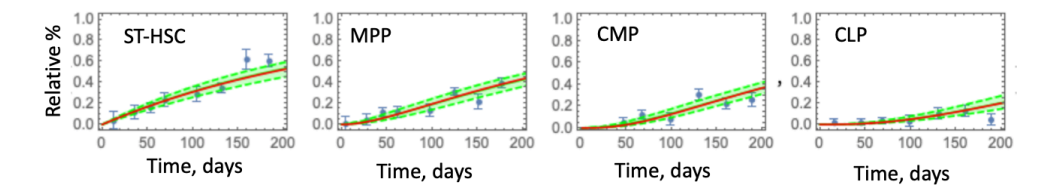


Figure S2: The relative proportions of the neutral label in the four compartments: ST-HSC, MPP, CLP, and CMP. Blue points show the data from \(\bar{\bar{\pi}} \) \(\bar{\pi} \), with error bars representing the standard error. The red curves are the best fits, and the green shaded areas represent the 95% confidence intervals of the fits.

 C_i . The corresponding system in then given by

$$\frac{dx_0}{dt} = r_0 x_0 (2p_0 - 1), (16)$$

$$\frac{dx_i}{dt} = 2r_{i-1}x_{i-1}(1-p_{i-1}) + r_ix_i(2p_i-1), \quad 1 \le i \le n-1, \quad (17)$$

$$\frac{dx_i}{dt} = 2r_{i-1}x_{i-1}(1-p_{i-1}) + r_ix_i(2p_i-1), \quad 1 \le i \le n-1, \quad (17)$$

$$\frac{dx_n}{dt} = 2r_{n-1}x_{n-1}(1-p_{n-1}) - d_nx_n. \quad (18)$$

Parameter d_3 in equation (18) (with n=3) was obtained as $d_3=(d_3^{(1)}\nu_3^{(1)}+d_3^{(2)}\nu_3^{(2)})/(\nu_3^{(1)}+\nu_3^{(2)})$. The best fit value is $d_3=0.0274~{\rm days^{-1}}$, with the 95% C.I. (0.015, 0.17).

1.2 The self-renewal probability functions and model calibration

In system (16–18), the quantity p_i is the probability of self renewal of cells in compartment C_i . We assume that these are functions of the cell populations. Most generally, we write

$$p_i = p_i(x_0, \dots, x_n), \quad 0 \le i \le n - 1.$$
 (19)

We will assume that these functions are such that a stable, positive steady state exists:

$$x_0(t) = X_0 > 0, \dots, x_n(t) = X_n > 0,$$

which is given by

$$X_{i} = X_{i-1} \frac{2r_{i-1}(1 - \bar{p}_{i-1})}{r_{i}(1 - 2\bar{p}_{i})} = X_{0} \prod_{m=1}^{i} \frac{2r_{m-1}(1 - \bar{p}_{m-1})}{r_{m}(1 - 2\bar{p}_{m})}, \quad 1 \le i \le n - 1, \quad (20)$$

$$X_n = \frac{2r_{n-1}(1-\bar{p}_{n-1})}{d_n}X_{n-1} \tag{21}$$

(note that $\bar{p}_0 = 1/2$).

The minimal requirements on the functions p_i are as follows:

- (i) Functions p_i are probabilities, that is, they satisfy $0 \le p_i \le 1$ for the relevant range of their arguments.
- (ii) The self-renewal probabilities are non-increasing functions of the downstream compartment as well as its own compartment, and they are non-decreasing functions of the upstream compartments (whenever applicable).

Here we will consider several special cases of the dependencies of p_i on cell populations. The first three examples below contain two constant nonnegative coefficients per function (those are denoted by c_i and h_i). The last example is characterized by a larger number of parameters.

1. Control from within each compartment, which we will refer to as "self' for a short-hand notation:

$$p_i = p_i(x_i), \quad 0 \le i \le n - 1.$$

For example, we will use the following functional form:

$$p_i = \frac{c_i}{1 + h_i x_i}. (22)$$

2. Control from the downstream compartment, which we will refer to as "next" for a short-hand notation:

$$p_i = p_i(x_{i+1}), \quad 0 \le i \le n-1.$$

An example is the following functional form:

$$p_i = \frac{c_i}{1 + h_i x_{i+1}}.$$

3. Control from the most differentiated compartment, which we will refer to as "last" for a short-hand notation:

$$p_i = p_i(x_n), \quad 0 \le i \le n - 1,$$

for example,

$$p_i = \frac{c_i}{1 + h_i x_n}$$

To satisfy constraint (i) above, we will assume that the functional form is relevant in some vicinity of the positive equilibrium, and away from the equilibrium the function is modified such that the probabilities are within [0, 1].

We note that the equilibrium compartment size, equations (20-21), does not depend on our choice of the control strength or type. The constraints on the control parameters come from the self-consistency requirements:

$$p_i(X_0, \dots, X_n) = \bar{p}_i, \quad 0 \le i \le n - 1.$$
 (23)

For the examples of functional forms studied here, if we assume certain values for all the control strength parameters such as h_i , equations (23) comprise a linear system system of n equations for n unknowns, c_0, \ldots, c_{n-1} . For the examples listed above, we have:

1. Control from within each compartment, "self":

$$c_0 = \frac{1}{2} + \frac{h_0 \bar{x}_0}{2}, \tag{24}$$

$$c_1 = \bar{p}_1 + \frac{r_0 \bar{x}_0 h_1 \bar{p}_1}{r_1 (1 - 2\bar{p}_1)}, \tag{25}$$

$$c_2 = \bar{p}_2 + \frac{2r_0\bar{x}_0h_2(1-\bar{p}_1)\bar{p}_2}{r_2(1-2\bar{p}_1)(1-2\bar{p}_2)}.$$
 (26)

2. Control from the downstream compartment, "next":

$$c_0 = \frac{1}{2} + \frac{h_0 r_0 \bar{x}_0}{2r_1 (1 - 2\bar{p}_1)}, \tag{27}$$

$$c_1 = \bar{p}_1 + \frac{2h_1\bar{p}_1r_0\bar{x}_0(1-\bar{p}_1)}{r_2(1-2\bar{p}_1)(1-2\bar{p}_2)}, \tag{28}$$

$$c_2 = \bar{p}_2 + \frac{4h_2\bar{p}_2r_0\bar{x}_0(1-\bar{p}_1)(1-\bar{p}_2)}{d_3(1-2\bar{p}_1)(1-2\bar{p}_2)}.$$
 (29)

3. Control from the most differentiated compartment, "last":

$$c_0 = \frac{1}{2} + \frac{2h_0r_0\bar{x}_0(1-\bar{p}_1)(1-\bar{p}_2)}{d_3(1-2\bar{p}_1)(1-2\bar{p}_2)},$$
(30)

$$c_1 = \bar{p}_1 + \frac{4h_1\bar{p}_1r_0\bar{x}_0(1-\bar{p}_1)(1-\bar{p}_2)}{d_3(1-2\bar{p}_1)(1-2\bar{p}_2)},$$
(31)

$$c_2 = \bar{p}_2 + \frac{4h_2\bar{p}_2r_0\bar{x}_0(1-\bar{p}_1)(1-\bar{p}_2)}{d_3(1-2\bar{p}_1)(1-2\bar{p}_2)}.$$
 (32)

Note that these expressions hold in the absence of control, when we simply set $h_i = 0$.

Figure $\boxed{3}$ illustrates convergence of the three control models to equilibrium $\boxed{20}$ - $\boxed{21}$), by showing the dynamics of the ODEs starting from a small number of cells in the LT-HSC compartment. In all simulations, we fixed control parameters h_i and used the above formulas for the parameters c_i . Panel (a) corresponds to the "self" control model, panel (b) to the "next" control model, and panel (c) to the "last" control model. We observe that all three models are capable of reaching the stable equilibrium (values X_0, \ldots, X_3 , equations $\boxed{20}$ - $\boxed{21}$), indicated by dashed horizontal lines in figure $\boxed{53}$). These simulations however are not meant to represent the process of development, where different types of feedback control are involved and different parameter values must be used for a realistic description.

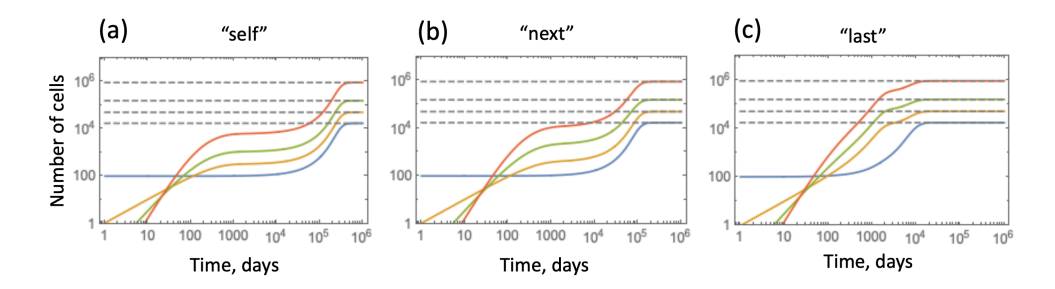


Figure S3: The ODE dynamics of the wild-type system for the three specific assumptions on the control of the self-renewal probabilities: (a) "self", (b) "next", and (c) "last". Populations shown are x_0 (blue), x_1 (yellow), x_2 (green), and x_3 (red). The initial conditions are $x_0(0) = 100$, $x_i(0) = 0$ for $i \ge 1$. The dashed horizontal lines are the equilibrium values, X_i , equations (20-21). $h = 10^{-7}$, and the rest of the parameters are as in table 1 of the main text.

2 Modeling wild-type and mutant co-dynamics

2.1 ODEs for wild type and mutant cells

In order to introduce mutations in the system, we denote by y_i the mutant population of compartment C_i , by $r_i^{(m)}$ the mutant division rates, and by $p_i^{(m)}$ the probabilities of self renewal for mutant cells in compartment C_i . Mutants can be generated upon cell division. The four possible division processes for wild type cells, in the presence of a per cell mutation rate u_i , are shown in figure [S4]. Mutants are assumed to divide into mutant daughter cells in the absence of back-mutations or additional mutations. The following set of ODEs describes the co-dynamics of wild type and mutant cells for n=3:

$$\dot{x}_{0} = r_{0}x_{0}p_{0}(1-u_{0}) - r_{0}x_{0}(1-p_{0}),$$

$$\dot{x}_{1} = r_{0}x_{0}(1-p_{0})(2-u_{0}) + r_{1}x_{1}p_{1}(1-u_{1}) - r_{1}x_{1}(1-p_{1}),$$

$$\dot{x}_{2} = r_{1}x_{1}(1-p_{1})(2-u_{1}) + r_{2}x_{2}p_{2}(1-u_{2}) - r_{2}x_{2}(1-p_{2}),$$

$$\dot{x}_{3} = r_{2}x_{2}(1-p_{2})(2-u_{2}) - d_{3}x_{3},$$

$$\dot{y}_{0} = r_{0}x_{0}p_{0}u_{0} + r_{0}^{(m)}y_{0}(2p_{0}^{(m)} - 1),$$

$$\dot{y}_{1} = r_{0}x_{0}(1-p_{0})u_{0} + 2r_{0}^{(m)}y_{0}(1-p_{0}^{(m)}) + r_{1}x_{1}p_{1}u_{1} + r_{1}^{(m)}y_{1}(2p_{1}^{(m)} - 1),$$

$$\dot{y}_{2} = r_{1}x_{1}(1-p_{1})u_{1} + 2r_{1}^{(m)}y_{1}(1-p_{1}^{(m)}) + r_{2}x_{2}p_{2}u_{2} + r_{2}^{(m)}y_{2}(2p_{2}^{(m)} - 1),$$

$$\dot{y}_{3} = r_{2}x_{2}(1-p_{2})u_{2} + 2r_{2}^{(m)}y_{2}(1-p_{2}^{(m)}) - d_{3}y_{3}.$$
(34)

In the absence of mutations $(u_i = 0)$, the general terms become:

$$\dot{x}_i = 2r_{i-1}x_{i-1}(1-p_{i-1}) + r_ix_i(2p_i-1),
\dot{y}_i = 2r_{i-1}^{(m)}y_{i-1}(1-p_{i-1}^{(m)}) + r_i^{(m)}y_i(2p_i^{(m)}-1).$$

In the above model we assume that the differences between wild type and mutant cells could be both in the division rate and in the self-renewal probability. Most generally, we write

$$p_i = p_i(x_0, y_0, \dots, x_n, y_n), \quad p_i^{(m)} = p_i^{(m)}(x_0, y_0, \dots, x_n, y_n), \quad 0 \le i \le n - 1.$$

A particular formulation that can be used assumes that the mutants' self-renewal probability is a multiple of that of wild-type cells:

$$p_i^{(m)} = (1+s)p_i,$$

where the constant s is the selection coefficient. Alternatively, mutants may be characterized by other differences in their self-renewal function compared to that of wild type cells, such as different control strength coefficients, h_i .

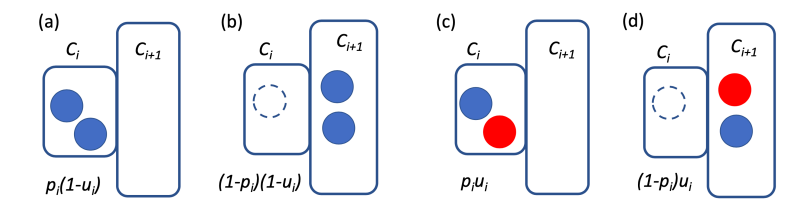


Figure S4: Four types of wild-type cell division: (a) faithful self-renewal, (b) faithful differentiation, (c) self-renewal with a mutation, (d) differentiation with a mutation. The compartments C_i and C_{i+1} are represented by rectangles, wild type cells by blue circles, mutants by red circles, and a position of a cell that has divided and differentiated by dashed circles. The per-cell probabilities of each cell division are indicated for each division type.

In what follows, we are interested in the invasion conditions for a mutant that has been introduced into different compartments in the absence of de novo mutant generation. Hence, we will assume $u_i = 0$ for the remainder of the analysis.

2.2 The mutant-free equilibrium and its stability

Consider the main system (33-34), under a general assumption on the control functions:

$$p_i = p_i(x_0 + y_0, x_1 + y_1, x_2 + y_2, x_3 + y_3),$$

$$p_i^{(m)} = p_i^{(m)}(x_0 + y_0, x_1 + y_1, x_2 + y_2, x_3 + y_3), \quad 0 \le i \le 2.$$

In the absence of de novo mutations $(u_i = 0, 0 \le i \le 2)$, a (positive) mutantfree solution is given by

$$\begin{pmatrix} x_0 \\ x_1 \\ x_2 \\ \frac{x_3}{y_0} \\ y_1 \\ y_2 \\ y_3 \end{pmatrix} = \begin{pmatrix} X_0 \\ X_1 \\ X_2 \\ \frac{X_3}{0} \\ 0 \\ 0 \\ 0 \end{pmatrix}, \quad X_i > 0, \quad 0 \le i \le 3, \tag{35}$$

where we used a horizontal bar to separate the wild type and mutant directions in the solution. This steady state satisfies the algebraic system of equations,

$$\frac{1}{2} = p_0(x_0, \dots, x_3), \tag{36}$$

$$x_1 = \frac{r_0 x_0}{r_1 (1 - 2p_1(x_0, \dots, x_3))}, \tag{37}$$

$$\frac{1}{2} = p_0(x_0, \dots, x_3), \tag{36}$$

$$x_1 = \frac{r_0 x_0}{r_1 (1 - 2p_1(x_0, \dots, x_3))}, \tag{37}$$

$$x_2 = \frac{2r_0 x_0 (1 - p_1(x_0, \dots, x_3))}{r_2 (1 - 2p_1(x_0, \dots, x_3)) (1 - 2p_2(x_0, \dots, x_3))}, \tag{38}$$

$$x_3 = \frac{4r_0 x_0 (1 - p_1(x_0, \dots, x_3)) (1 - p_2(x_0, \dots, x_3))}{d_3 (1 - 2p_1(x_0, \dots, x_3)) (1 - 2p_2(x_0, \dots, x_3))}, \tag{39}$$

$$y_i = 0, \quad 0 < i < 3. \tag{40}$$

$$x_3 = \frac{4r_0x_0(1 - p_1(x_0, \dots, x_3))(1 - p_2(x_0, \dots, x_3))}{d_3(1 - 2p_1(x_0, \dots, x_3))(1 - 2p_2(x_0, \dots, x_3))},$$
(39)

$$y_i = 0, \quad 0 \le i \le 3.$$
 (40)

This system simplifies for our three examples, $p_i = p_i(x_i)$, or $p_i = p_i(x_{i+1})$, or $p_i = p(x_3)$. An explicit solution, if available, will depend on the form of the control functions.

One can investigate stability properties of mutant-free solution (35) by analyzing system (33-34) with $u_i = 0$. Note that the analysis below is presented for n=3 but is generalized easily to other numbers of compartments,

Following the standard technique, we write out the Jacobian of the system evaluated at the equilibrium, and determine its eight (2(n+1)) eigenvalues, λ_i , $0 \le i \le 7$. It turns out that there are two distinct groups of eigenvalues. Eigenvalues $\lambda_4, \ldots, \lambda_7$ do not depend on the mutant parameters, and the

corresponding eigenvectors have zero projections on the 4 mutant directions:

$$\mathbf{v}^{(i)} = \begin{pmatrix} * \\ * \\ * \\ 0 \\ 0 \\ 0 \\ 0 \end{pmatrix}, \quad 4 \le i \le 7, \tag{41}$$

where stars denote solution components that are not identically zero. The top n+1 components here correspond to the $x_0, \ldots x_3$ directions and the bottom n+1 components to the y_0, \ldots, y_3 directions, so the eigenvectors in this group only have nontrivial components corresponding to wild-type populations. While the functional shape of the eigenvalues $\lambda_4, \ldots, \lambda_7$ and their eigenvectors depends on the control functions, generally they describe the stability of the positive mutant-free equilibrium in the absence of mutants and can be obtained from the Jacobian of system [16-18]. Here we assume that they have a negative real part, that is, a positive equilibrium is stable in the absence of mutants.

The rest of the eigenvalues have a simple form:

$$\lambda_i = r_i^{(m)} (2p_{i,eq}^{(m)} - 1), \quad 0 \le i \le 2,$$
 (42)

$$\lambda_3 = -d_3, \tag{43}$$

where $p_{i,eq}^{(m)}$ denotes the function $p_i^{(m)}(X_0, X_1, X_2, X_3)$ evaluated at the mutant-free equilibrium. The corresponding eigenvectors have the following form:

$$\mathbf{v}^{(0)} = \begin{pmatrix} * \\ * \\ * \\ * \\ * \\ * \\ * \end{pmatrix}, \ \mathbf{v}^{(1)} = \begin{pmatrix} * \\ * \\ * \\ * \\ 0 \\ * \\ * \end{pmatrix}, \ \mathbf{v}^{(2)} = \begin{pmatrix} * \\ * \\ * \\ * \\ 0 \\ 0 \\ 0 \\ * \\ * \end{pmatrix}, \ \mathbf{v}^{(3)} = \begin{pmatrix} * \\ * \\ * \\ 0 \\ 0 \\ 0 \\ 0 \\ * \end{pmatrix},$$

$$(44)$$

where again, the stars denote solution components that are not identically zero. We can see that for the eigenvector corresponding to eigenvalue λ_i with

 $0 \le i \le 3$, the mutant populations in the compartments upstream from i (if applicable) are zero.

From the expressions for the eigenvalues, (42-43), we can see that the mutant division rates (as long as they are positive) do not influence stability. Instead, conditions that guarantee stability of mutant-free solutions involve mutant self-renewal probabilities:

$$p_{i,eq}^{(m)} < 1/2, \quad 0 \le i \le 2.$$
 (45)

In other words, mutant cells can invade if in at least one of the compartments, they are capable of self-renewal, that is, their self-renewal probability at the wild-type equilibrium exceeds their differentiation probability.

This analysis can be used to examine the fate of mutants originating in different compartments. Still keeping all the mutation rates at zero, assume that mutant production in a given compartment is incorporated through the initial condition:

$$y_i(0) = \begin{cases} \hat{y} > 0, & i = k, \\ 0, & i \neq k, \end{cases}$$
 (46)

where k is the compartment where the mutation originates. Whether or not this destabilizes the mutant-free solution and leads to a spread of mutants can be determined by examining the relevant solutions of the linear system.

The solution of the linearized system (33-34) with $u_i = 0$ describes the dynamics of the perturbation and is written in the standard form,

$$\sum_{j=0}^{7} \alpha_j \mathbf{v}^{(j)} e^{\lambda_j t}, \tag{47}$$

where the coefficients α_i are obtained from the initial condition,

$$(0,0,0,0,y_0(0),y_1(0),y_2(0),y_3(0))^T$$
,

given by (46). Since by our assumption, $\lambda_j < 0$ for $4 \le j \le 7$, the fate of the perturbation (that is, whether or not the mutant will grow) is defined by the first four terms in this sum.

For mutants originating in C_0 (that is, k=0 in (46)), in general we expect nontrivial values of α_j for all $0 \le j \le 3$. In particular, notice that the only eigenvector (out of the eight of them) that has a nontrivial component corresponding to y_0 is $\mathbf{v}^{(0)}$, see expressions (41) and (44). Therefore, the first coefficient α_0 is obtained from $\alpha_0 v_4^{(0)} = \hat{y}$ (where $v_j^{(i)}$ denotes the jth

component of eigenvector $\mathbf{v}^{(i)}$ with $0 \leq j \leq 7$). The second coefficient satisfies $\alpha_0 v_5^{(0)} + \alpha_1 v_5^{(1)} = 0$, etc. Since all the terms in (47) come with nonzero coefficients, all the values in (42) must be negative for stability of the mutant-free state. This means that as long as any of the three inequalities in (45) are violated, the mutant can invade.

The situation is different for mutants placed in downstream compartments. For mutants originating in C_1 (k=1 in (46)), we obtain $\alpha_0 v_4^{(0)}=0$, such that $\alpha_0=0$. Then we have $\alpha_1 v_5^{(1)}=\hat{y}$, and the rest of the coefficients α_j have nontrivial values. This means that the initial condition does not have a nontrivial projection onto the eingenvector corresponding to λ_0 in (42), therefore, only two out of the three conditions in (49) apply, namely, the ones with i=1 and i=2. Consequently, to destabilize the mutant-free solution, one must satisfy the weaker of the two conditions, $p_{i,eq}^{(m)} > 1/2$, i=1,2.

For mutants originating in C_2 , we have $\alpha_0 = \alpha_1 = 0$, and only the i = 2 condition in (42) is relevant. Therefore, to destabilize the mutant-free solution, one must have $p_{2,eq}^{(m)} > 1/2$.

2.3 Fitness thresholds for mutant invasion

Let us consider the special case where the mutant self-renewal probability in each compartment is given by

$$p_i^{(m)} = (1+s)p_i, \quad 0 \le i \le 2. \tag{48}$$

The quantity s can be positive, zero, or negative, and it can be interpreted as a selection coefficient. Then, stability conditions (45) can be rewritten as

$$(1+s)\bar{p}_i < 1/2, \quad 0 \le i \le 2.$$
 (49)

If $\bar{p}_0 = 1/2$ and $\bar{p}_i < 1/2$ for i = 1 and i = 2, any positive value of s will destabilize the mutant-free solution. Under the assumption in (48), mutant invasion conditions can be formulated as a threshold result. Let us suppose that, in the absence of further de-novo mutations, mutants are placed in compartment k, equation (46). Then the mutant invasion conditions become:

$$s > s_c = \min\left\{\frac{1}{2\bar{p}_k} - 1, \dots, \frac{1}{2\bar{p}_{n-1}} - 1\right\},$$
 (50)

that is, the invasion threshold is determined by the equilibrium self-renewal probability in compartment k and all the compartments downstream from it. To summarize: if a mutant is generated in the least differentiated compartment (C_0) then any positive value of s is sufficient for the mutant to be advantageous (and invade in the deterministic system). If however the mutant originates in one of the downstream compartments, there is a nontrivial threshold value that s must exceed to be able to invade. For a mutant that originates in compartment C_k , the size of the threshold is defined by the largest of the \bar{p}_l values with $l \geq k$, equation (50).

With n=3, there are two cases depending on the relative magnitudes of \bar{p}_1 and \bar{p}_2 . If the equilibrium self-renewal probabilities satisfy

$$1/2 = \bar{p}_0 > \bar{p}_2 > \bar{p}_1, \tag{51}$$

we have the following mutant invasion thresholds:

$$s > s_c = \begin{cases} 0, & k = 0, \\ \min\left\{\frac{1}{2\bar{p}_1} - 1, \frac{1}{2\bar{p}_2} - 1\right\} = \frac{1}{2\bar{p}_2} - 1, & k = 1, \\ \frac{1}{2\bar{p}_2} - 1, & k = 2. \end{cases}$$
 (52)

This means that for mutants originating in either of the compartments C_1 or C_2 , the same invasion threshold exists, which is the lower of the two values.

If, consistent with Table 1 of the main text,

$$1/2 = \bar{p}_0 > \bar{p}_1 > \bar{p}_2, \tag{53}$$

then

$$s > s_c = \begin{cases} 0, & k = 0, \\ \min\left\{\frac{1}{2\bar{p}_1} - 1, \frac{1}{2\bar{p}_2} - 1\right\} = \frac{1}{2\bar{p}_1} - 1, & k = 1, \\ \frac{1}{2\bar{p}_2} - 1, & k = 2. \end{cases}$$
 (54)

In other words, mutants that originate further downstream will face a higher threshold compared to those that originate lower. It is reasonable to assume that the likelihood of mutant generation in C_2 is higher than that for C_1 , because of the larger size of C_2 . It therefore appears that the architecture with $\bar{p}_2 < \bar{p}_1$ presents a higher degree of protection against mutant invasion compared to the case with $\bar{p}_1 < \bar{p}_2$.

The value of the self-renewal probability at the equilibrium is responsible for the compartment size: the closer this value is to 1/2, the larger the compartment size (see figure $\overline{S5}(a)$, where this is illustrated using compartment C_2). Therefore, from the point of view of cell amplification in tissue, it is important to keep this quantity closer to 1/2. On the other hand, as this analysis shows, values of \bar{p}_i close to 1/2 tend to lower the mutant invasion threshold for mutants that originate in the given compartment (or even in compartments upstream from that, see figure $\overline{S5}(b)$). Therefore, there is a certain trade-off between the functionality and protection against mutations, where the values of self-renewal probability play a pivotal role.

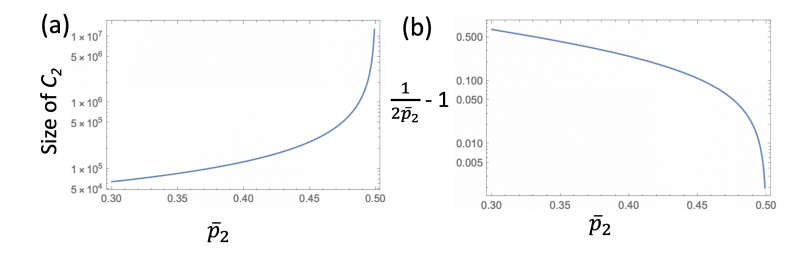


Figure S5: Compartment size (a) and mutant invasion threshold (b) as functions of the equilibrium self-renewal probability \bar{p}_2 . The rest of the parameters are given in table 1 of the main text.

3 The fate of mutants originating in different compartments

In what follows we study how mutants originating in different compartments, may spread through the systems, and how the dynamics depend on the type of control, the strength of the control and the amount of advantage enjoyed by the mutant. We assume that the mutation rate is low, such that once a mutant appears, no new mutations are considered.

3.1 Mutants originating in C_0 : pure mutant solutions

Since no de-differentiation is assumed in the model, the only way a mutant can occupy compartment C_0 is to be generated there. From compartment C_0 ,

it can spread to all the downstream compartments. In addition, mutants that originate in downstream compartments, also contribute to the dynamics. If a mutant has an advantage in compartment C_0 ($p_{0,eq}^{(m)} > 1/2$) then a purelymutant solution is established, where the mutants displace the wild-type in C_0 and consequently, in all the compartments.

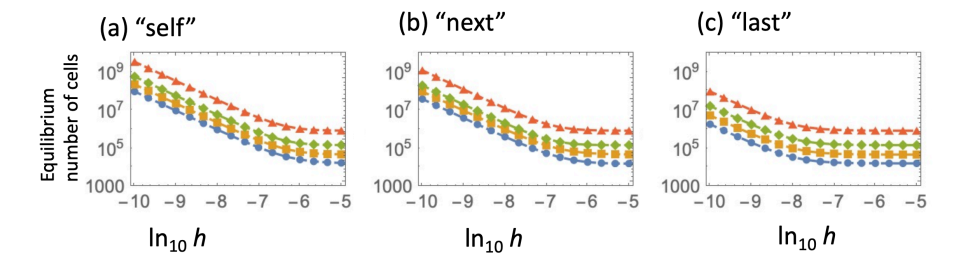


Figure S6: The dependence of the pure mutant equilibrium on the control type and the control strength: (a) "self", (b) "next", and (c) "last" type of control. For each type of control, the equilibrium quantities $(y_0 \text{ (blue)}, y_1 \text{ (yellow)}, y_2 \text{ (green)}, y_3 \text{ (red)})$ are plotted as functions of $\ln_{10} h$, where $h_i = h$ for all i is control strength. Mutant selection coefficient is s = 0.01. The rest of the parameters are given in table 1 of the main text.

While the equilibrium values for the wild-type cells are identical in all of our models of control, mutant behavior depends on both the type of the control functions, and on the strength of control. Figure 56 demonstrates how the pure mutant equilibrium values depend on the strength of control (assuming for simplicity $h_i = h$ for $0 \le i \le 2$) for the three types of control system. Generally, the cell numbers for the mutants increase as control decreases, and the solution diverges as $h \to 0$.

Figure S7 shows an example of wild-type (solid) and mutant (dashed) co-dynamics, for different control types (rows) and strengths (columns). The initial condition in each simulation is $y_0(0) = 1$ with other mutant values being zero at the beginning, and the wild-type values set at the mutant-free equilibrium, $x_i(0) = X_i$, $0 \le i \le 3$. As time goes by, we observe that the wild type cells are displaced by mutants. Even though the initial mutant placement is in C_0 , the compartments turn mutant in the reverse order, from C_3 and then C_2 , followed by C_1 and finally C_0 . This is the consequence of the increasing division rates from least to most differentiated compartments.

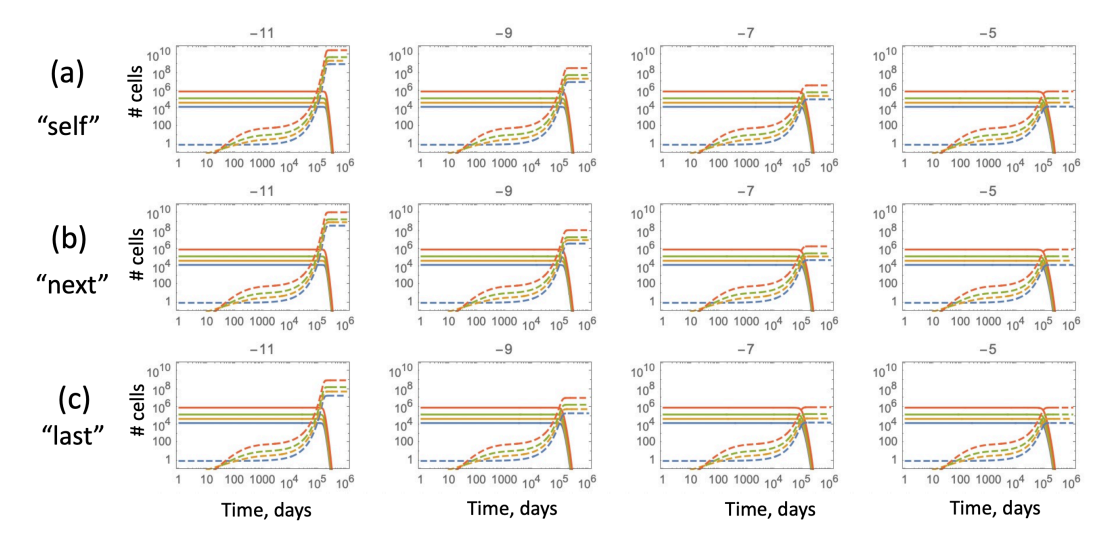


Figure S7: The dynamics of advantageous mutants introduced in C_0 . The wild type cells (solid lines) and the mutants (dashed lines) in compartments C_0 (blue), C_1 (yellow), C_2 (green), and C_3 (red) are plotted as functions of t under the (a) "self", (b) "next", and (c) "last" type of control. The different panels in each row correspond to different control strengths, with the quantity $\ln_{10} h$ marked above each plot. s = 0.01, $u_i = 0$ for all i, and the rest of the parameters are given in table 1 of the main text.

3.2 Mutants originating in downstream compartments

As was mentioned previously, if a mutant originates in compartment C_0 , under any positive value of s it will act as an advantageous mutant. The situation is different if the mutant originates in one of the downstream compartments. In order to destabilize the mutant-free solution, that is, in order to invade the WT population at equilibrium, the mutant must grow from low numbers. For that to occur, the initial mutant self-renewal rate must be greater than its differentiation rate. Under model (48) this translates to a threshold condition for the selection coefficient s. For the parameters of table 1 of the main text, we have

$$s_c^{(1)} \equiv \frac{1}{2\bar{p}_1} - 1 \approx 0.058, \quad s_c^{(2)} \equiv \frac{1}{2\bar{p}_2} - 1 \approx 0.203.$$

Since the self-renewal rates satisfy inequality (53), the invasion thresholds are given by (54). Simulations below demonstrate this result.

In figures $\overline{S8}$ and $\overline{S9}$, the mutant introduced in C_1 and has selection

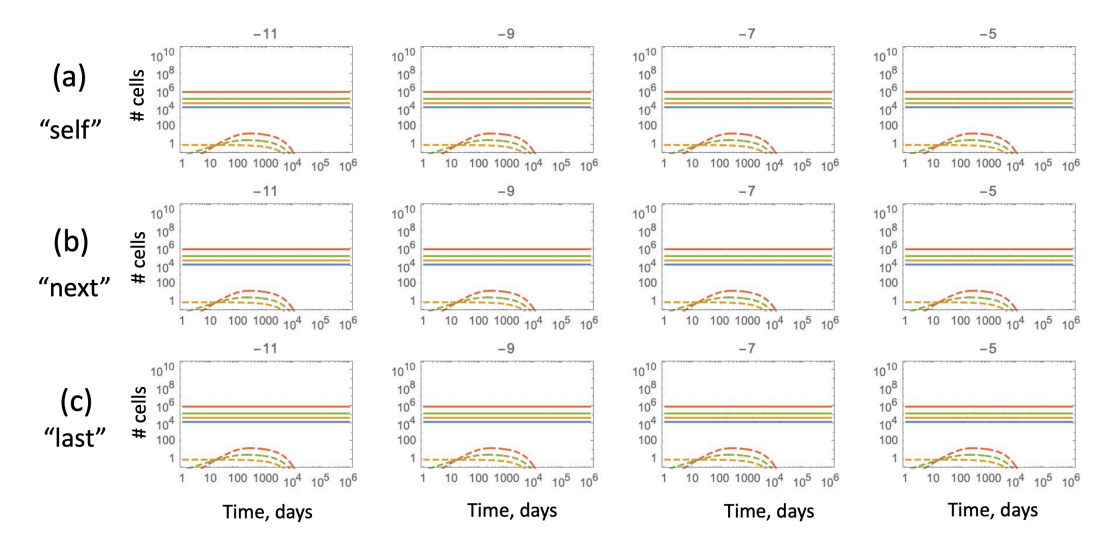


Figure S8: The dynamics of advantageous mutants (s = 0.05) introduced in C_1 . Mutant fitness is below the threshold: $s < s_c^{(1)} \approx 0.058$. The notations and the rest of the parameters are as in figure S7.

coefficient s = 0.05 and s = 0.06, respectively. In figure S8, we have $s < s_c^{(1)}$, that is, the selection coefficient is below the threshold in C_1 . As a result, the mutant dies out in its compartment of origin $(C_1, \text{ yellow dashed lines})$ and is unable to spread. In contrast to this, in figure S9 we have $s_c^{(2)} > s > s_c^{(1)}$, that is, the selection coefficient exceeds the threshold in C_1 , and a mutant population gets established in C_1 . Even though the threshold for compartment C_2 is not reached by these mutants, the existence of the input from C_1 makes the threshold in C_2 irrelevant, and the mutants subsequently spread to the downstream compartments.

As with mutants originating in C_0 , the steady state level of successfully spreading mutants depends on the strength of the feedback, measured by h here. For high h (strong feedback) the mutants' equilibrium is lower than the wild-type equilibrium in the respective compartments (see the rightmost panels in figure 59). For weaker values of feedback, the equilibrium value of the mutants grows (and diverges for $h \to 0$).

Figure $\overline{S9}$ demonstrates another difference compared to mutants originating in C_0 : in cases where the mutant is introduced in C_1 , the resident wild-type population is not necessarily driven extinct by the expanding mutant,

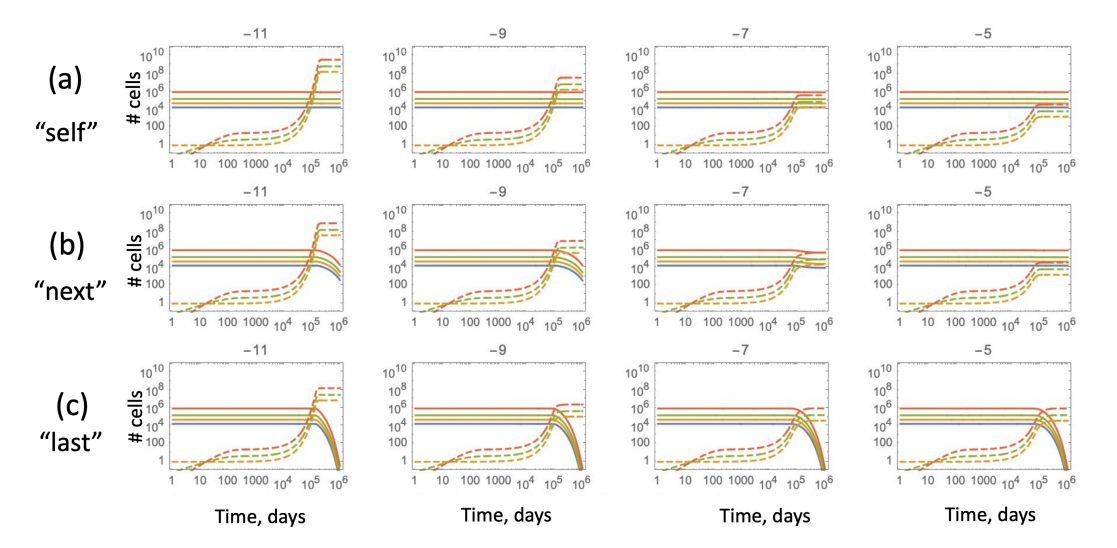


Figure S9: The dynamics of advantageous mutants (s = 0.06) introduced in C_1 . Mutant fitness is above the threshold: $s > s_c^{(1)} \approx 0.058$. The notations and the rest of the parameters are as in figure S7.

resulting in coexistence steady states. The fate of wild-type cells depends on the model formulation for the control of self-renewal probabilities. In the model where the control is "self" type (panel (a)), the wild type populations remain constant and the mutants grow to their equilibrium values. If the feedback is of type "next" or "last" (panels (b) and (c)), the wild-type populations may become decreased or go extinct in the presence of mutants.

The timing of mutant invasion depends on the amount of mutant advantage. Figure $\boxed{\$10}$ compares the dynamics of mutants with s=0.2 (significantly over the invasion threshold in C_1) with those with s=0.06 (just above the threshold, depicted in figure $\boxed{\$9}$). Apart from an enormous acceleration in the mutant rise in all models, we also observe a higher level of the mutant equilibrium.

If mutants originate in C_2 , under the parameter values of Table 1 of the main text, they have a much higher threshold to overcome. If the value $s < s_c^{(2)}$, the mutants will die out. Figure S11 shows mutants with s = 0.21, just above the threshold. These mutants successfully spread. The patterns of dependence on the feedback structure and strength are similar to what was noted above.

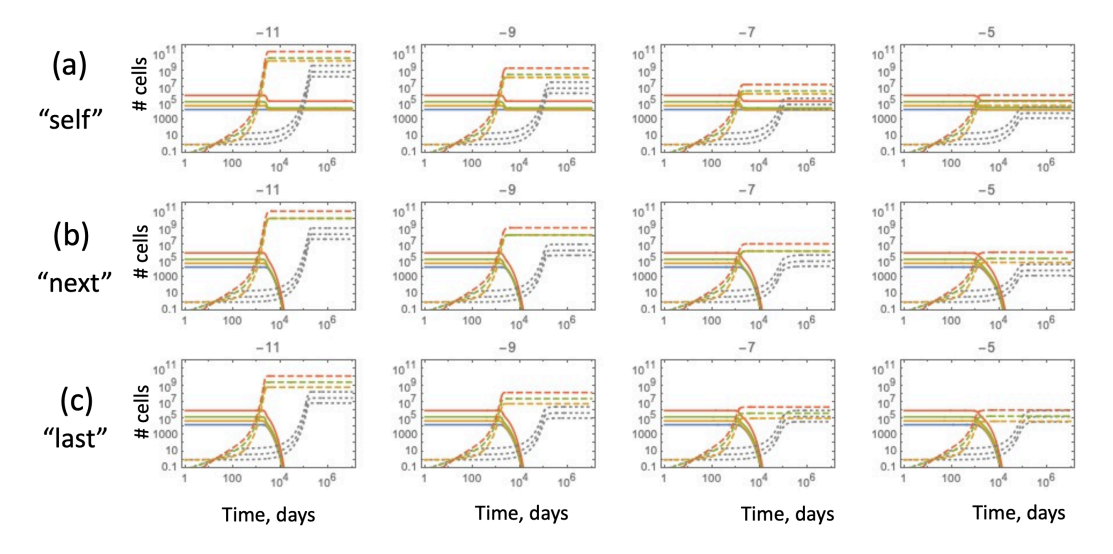


Figure S10: The dynamics of advantageous mutants with a larger fitness (s = 0.2, compared to figure S9) introduced in C_1 . The mutant numbers under the assumption of s = 0.06 (same as those in figure S9) are shown in dotted gray lines, for comparison. The notations and the rest of the parameters are as in figure S7.

3.3 Control of "self" type, mutants originating in C_1 : a case study

Here we examine a specific system with mutants originating in C_1 , and focus our attention on the equilibria in that compartment. In the absence of mutations, we have for C_1 :

$$\dot{x}_1 = r_0 x_0 + r_1 x_1 (2p_1 - 1), \tag{55}$$

$$\dot{y}_1 = r_1 y_1 (2(1+s)p_1 - 1);$$
 (56)

note that we took $p_0(x_0) = 1/2$, which remains constant in this model, where $p_i = p_i(x_i + y_i)$. It is useful to write down the Jacobian of the system:

$$J = \begin{pmatrix} r_1(2p_1 - 1) + 2r_1x_1p_1' & 2r_1x_1p_1' \\ 2r_1y_1(1+s)p_1' & r_1(2(1+s)p_1 - 1) + 2r_1y_1(1+s)p_1' \end{pmatrix}. (57)$$

If $x_0p_0 > 0$, there are two steady state solutions, discussed below.

The mutant-free solution: $y_1 = 0$, and x_1 is given by

$$x_1 = \frac{r_0 x_0}{r_1 (1 - 2\bar{p}_1)}. (58)$$

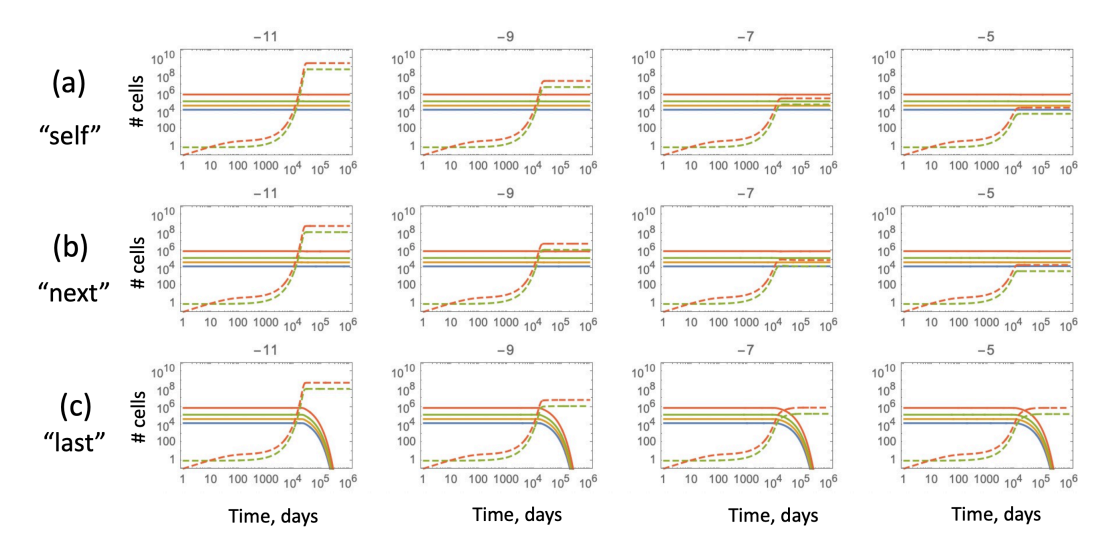


Figure S11: The dynamics of advantageous mutants (s=0.21) introduced in C_2 . Mutant fitness is above the threshold: $s>s_c^{(2)}\approx 0.203$. The notations and the rest of the parameters are as in figure $\boxed{\$7}$.

The eigenvalues of the corresponding Jacobian are $r_1(2p_1-1)+2rx_1p'_1$ and $r_1(2(1+s)p_1-1)$, evaluated at the steady state. This solution is stable when $(1+s)p_1 < 1/2$, and becomes unstable if $(1+s)\bar{p}_1 > 1/2$. As the value of s grows, the system experiences a transcritical bifurcation at

$$s = s_c = \frac{1}{2\bar{p}_1} - 1. (59)$$

As explained for the general case, for $0 < s < s_c$, mutants, although having a positive selection coefficient, effectively behave as disadvantageous mutants. The threshold value is higher if \bar{p}_i is further from 1/2.

Mutant solution:
$$y_1 > 0, x_1 > 0, (1+s)p_1(x_1, y_1) = 1/2$$
, and
$$x_1 = \frac{r_0 x_0 (1+s)}{r_1 s}.$$
 (60)

The number of wild type cells is independent of control, but the number of mutants depends strongly on control, increasing as the control parameter becomes weaker. This solution becomes stable when s is greater than critical

 $(s > s_c)$. This solution is characterized by mutants that are able to maintain their numbers in the compartment, through a sufficiently high value of s. For the particular shape of control defined in (22), the steady state is given by equation (60) and

$$y_1 = \frac{(2\bar{p}_1(1+s) - 1)(r_1s(2\bar{p}_1 - 1) - h_1r_0x_0(1+s))}{h_1r_1s(2\bar{p}_1 - 1)}.$$
 (61)

While x_1 is independent of control, y_1 depends strongly on h_1 . There are two distinct regimes, separated by the value h_c ,

$$h_c = \frac{sr_1(1 - 2\bar{p}_1)}{r_0x_0(1+s)}.$$

• Weak control. If $h_1 \ll h_c$, we have

$$y_1 \approx \frac{2\bar{p}_1(1+s) - 1}{h_1},$$
 (62)

that is, it is inversely proportional to control parameter h_1 , and tends to infinity in the absence of control $(h_1 \to 0)$.

• Strong control. If $h_1 \gg h_c$, we have a constant (h_1 -independent) level of mutants,

$$y_1 \approx \frac{r_0 x_0 (1+s)(2\bar{p}_1 (1+s) - 1)}{r_1 s(2\bar{p}_1 - 1)}.$$
 (63)

Figure S12 shows the behavior of solution (61) and its approximations.

3.4 Threshold conditions and stochastic modeling

In this section we return to the scenario described by inequalities (51), that is, to the situation where the threshold in compartment C_1 is higher than that in compartment C_2 . In the deterministic description of ODEs, a mutant that appears in compartment C_1 (that is, $y_1(0) > 0$) will immediately give rise to a nontrivial value of y_2 by the process of differentiation. This is why mutant cells that are generated in C_1 and do not satisfy the threshold condition in the compartment of their origin, will still make it to the next compartment (C_2) , and if they exceed the threshold there, they will rise and destabilize the mutant -free solution, see threshold condition (52).

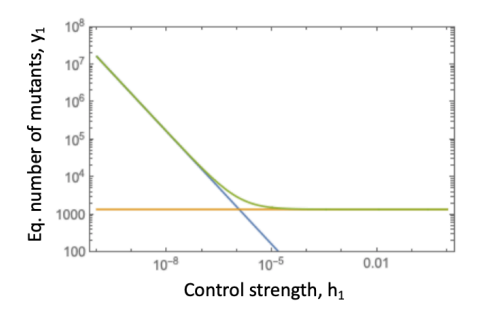


Figure S12: The equilibrium number of mutants (originating in C_1), equation (61), green, as a function of the control strength, h_1 . Blue and orange lines represent approximations (62) and (63), respectively. Here s = 0.06, and the rest of the parameters are given in table 1 of the main text.

A different scenario can occur if (i) there is a nonzero probability of cell death in C_1 , and (ii) the system is stochastic. In this case, it is possible that mutants (that act as disadvantageous mutants in C_1 because their selection coefficient is below the threshold), may die out before they make it to C_2 (where they are advantageous) by differentiation. A single one of the two modifications, (i) or (ii), is not sufficient to observe this scenario, but the combination may lead to this outcome. Specifically, in a stochastic system without cell death, mutant cells in C_0 will make it to C_1 because they can only self-renew or differentiate, so they cannot disappear from C_1 without exiting to C_2 . In a deterministic system with death, a nontrivial term is still present in the equation for y_2 , as long as y_1 is positive. Therefore, both (i) and (ii) have to be implemented to see a change in the behavior. Below we investigate the resulting system, to calculate the probability that a mutant in C_1 differentiates into C_2 before dying out.

Consider the dynamics of mutant cells originating in compartment C_1 , in the absence of further mutations (similar analysis can also be used for mutants that originate in more differentiated compartments, such as C_2). Denote the number of mutants by i and the total number of cells in C_1 as N. We will represent the dynamics as a Gillespie-type process, where we focus on the changes in the variable i. We are interested in finding the probability that mutant cells in compartment C_1 differentiate (that is, send mutants to compartment C_2), before they die off in compartment C_1 . The state space consists of the values $i \in \{E, 0, 1, \ldots\}$, where the additional state E stands

for the event where a mutant cell differentiated into C_2 . Both state i = 0 and i = E are absorbing. Table [S1] lists all the processes and their propensities. In what follows we assume that $i \ll N$ and ignore fluctuations in the number

Event	Propensity
W.t. cell division	$(N-i)r_1$
W.t. cell differentiation from C_0	x_0r_0
W.t. death	$(N-i)d_1$
Mutant self-renewal, $i \to i+1$	$ir_1p_1^{(m)}$
Mutant death, $i \to i-1$	id_1
Mutant differentiation, $i \to E$	$ir_1(1-p_1^{(m)})$
Total	$\mathcal{N} \equiv x_0 r_0 + N(r_1 + d_1)$

Table S1: Mutant and wild type processes and their propensities in compartment C_1 .

of wild type cells. Therefore, $p_1^{(m)}$, which is a function of both the number of wild type and mutant cells, can be approximated by its equilibrium value, $(1+s)\bar{p}_1$. Envisage the stochastic process where at each time-step of length Δt , the following events are possible:

$$P(i \to i+1) = \frac{ir_1 p_1^{(m)}}{\mathcal{N}} \Delta t, \tag{64}$$

$$P(i \to i - 1) = \frac{id_1}{\mathcal{N}} \Delta t, \tag{65}$$

$$P(i \to E) = \frac{ir_1(1 - p_1^{(m)})}{\mathcal{N}} \Delta t, \tag{66}$$

$$P(i \to i) = 1 - (P(i \to i+1) + P(i \to i-1) + P(i \to E)).$$
 (67)

For the usual Gillespie algorithm, for each step, one would choose the next process according to the events' propensities and then calculate the time interval as a random exponentially distributed variable. Here we are interested in the probability for the mutant cells to make it (by differentiation) to the next compartment, so we will not focus on the timing of events, only on their sequence. Denote by g_i the probability of absorbing in state E starting from state i. We have

$$g_i = P(i \to E) + P(i \to i+1)g_{i+1} + P(i \to i-1)g_{i-1} + P(i \to i)g_i, \quad i \ge 1, \quad g_0 = 0.$$

This can be simplified to

$$c + ag_{i+1} + bg_{i-1} - (a+b+c)g_i = 0, \quad i \ge 1,$$

where

$$a = r_1 p_1^{(m)}, \quad b = d_1, \quad c = r_1 (1 - p_1^{(m)}).$$

Denoting $q_i = 1 - g_i$, we obtain the system

$$cq_i = a(q_{i+1} - q_i) + b(q_{i-1} - q_i), \quad i \ge i, \quad q_0 = 1,$$

which can be solved by the substitution $q_i = \alpha^i$. The values of α are obtained as the roots of a quadratic equation.

$$\alpha_{1,2} = \frac{a+b+c \pm \sqrt{(a+b+c)^2 - 4ab}}{2a}.$$

The solution is $q_i = A\alpha_1^i + B\alpha_2^i$, and the constants A and B are found from the conditions $q_0 = 1$ and $0 \le q_i \le 1$ (because g_i is a probability). It is easy to show that $\alpha_1 > 1$ and $0 < \alpha_2 < 1$. Therefore, we need to set A = 0 and B = 1. Finally, we obtain the probability for mutants to differentiate before dying out in C_1 , starting from a single cell:

$$g_1 = 1 - \frac{1 - \sqrt{1 - \nu \mu}}{\nu},$$

where

$$\nu = \frac{2a}{a+b+c} = \frac{2r_1p_1^{(m)}}{r_1+d_1}, \quad \mu = \frac{2b}{a+b+c} = \frac{2d_1}{r_1+d_1}.$$

We have

$$\frac{\partial g_1}{\partial \nu} < 0, \quad \frac{\partial g_1}{\partial \mu} < 0.$$

Using this information, we can see that g_1 decreases with $p_1^{(m)}$, which is expected: the more often the cells self-renew, the less often they differentiate, making it less likely for mutants to "escape" to the next compartment before dying out. We also see that if $d_1 = 0$, then $g_1 = 1$, again, as expected. Finally, we can calculate the derivatives:

$$\frac{\partial g_1}{\partial d_1} = \frac{d_1 + r_1(1 - 2p_1^{(m)}) - \sqrt{(d_1 + r_1(1 - 2p_1^{(m)}))^2 + 4(1 - p_1^{(m)})r_1^2}}{2p_1^{(m)}r_1\sqrt{(d_1 + r_1(1 - 2p_1^{(m)}))^2 + 4(1 - p_1^{(m)})r_1^2}} < 0,$$

$$\frac{\partial g_1}{\partial r_1} = -\frac{d_1}{r_1}\frac{\partial g_1}{\partial d} > 0,$$

where $p_1^{(m)} = (1+s)\bar{p}_1$. We conclude that increasing the division rates or decreasing the death rates will increase the probability of "escape".

4 Including replication limits in the lineage dynamics

4.1 The wild type system

Let us suppose that LT-SCs can divide indefinitely, but cells in the downstream compartments have a replication limit, which we call K. Accordingly, for compartments C_i with i = 1 and i = 2, we will split all cells in division classes, such that $x_1 = \sum_{k=1}^K x_{1k}$, $x_2 = \sum_{k=1}^K x_{2k}$; here the second index, k, enumerates the division classes, while the first index stands for the compartment number. We will assume that cells differentiate from compartment C_0 into compartment C_1 by entering class x_{11} . For divisions in class x_{ik} , at each cell division, the progeny is placed in class $x_{i,k+1}$ with probability p_i (a self-renewal division), and in class $x_{i+1,k+1}$ with probability $1 - p_i$ (a differentiation division). We assume that the progeny of cells in classes x_{iK} is removed from the system. The following of ODEs describes these processes:

$$C_{0}: \dot{x}_{0} = r_{0}x_{0}(2p_{0}-1), (68)$$

$$C_{1}: \dot{x}_{11} = 2r_{0}x_{0}(1-p_{0}) - r_{1}x_{11}, \dot{x}_{1k} = 2r_{1}x_{1,k-1}p_{1} - r_{1}x_{1k}, 2 \leq k \leq K,$$

$$C_{2}: \dot{x}_{21} = -r_{2}x_{21}, \dot{x}_{22} = 2r_{1}x_{11}(1-p_{1}) - r_{2}x_{22}, \dot{x}_{2k} = 2r_{1}x_{1,k-1}(1-p_{1}) + 2r_{2}x_{2,k-1}p_{2} - r_{2}x_{2k}, 3 \leq k \leq K.$$

$$C_{3}: \dot{x}_{3} = 2r_{2}\sum_{k=1}^{K} x_{2k}(1-p_{2}) - d_{3}x_{3}. (69)$$

We will assume, as before, that the probabilities of self-renewal are functions of the quantities x_i , $i \in \{0, 1, 2, 3\}$. At the equilibrium, we have $p_i = \bar{p}_i$, with

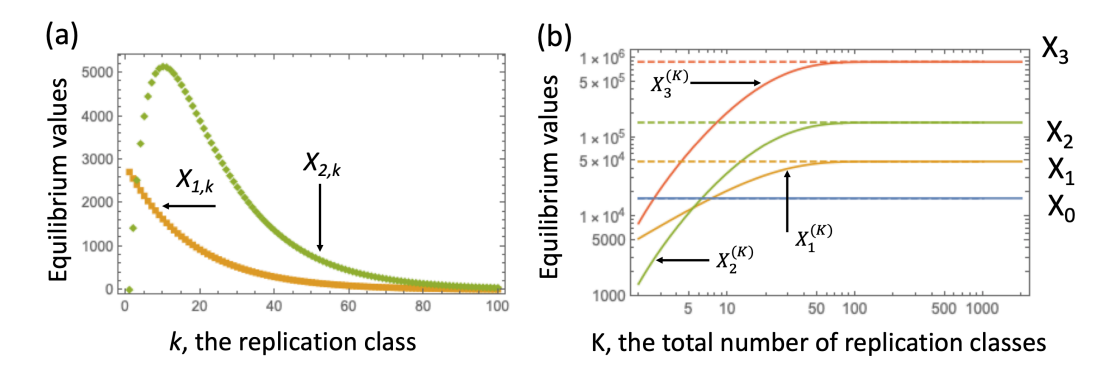


Figure S13: Equilibrium solutions for the system with replication limits. (a) Equilibrium values in the individual replication classes, $X_{1,k}$ and $X_{2,k}$, equations (71,72). (b) The equilibrium values of the cell populations in the 4 compartments as functions of the total number of replication classes, K. The horizontal dashed lines show the equilibrium values for the basic system in the absence of replication limits, equations (20,21).

 $\bar{p}_0 = 1/2$. The equilibrium solution is then given by:

$$X_0 = \bar{x}_0, \tag{70}$$

$$X_{1,k} = \frac{r_0 \bar{x}_0}{r_1} (2\bar{p}_1)^{k-1}, \quad 1 \le k \le K, \tag{71}$$

 $X_{2,1} = 0,$

$$X_{2,k} = \frac{r_1}{r_2} X_{11} 2^{k-1} (1 - \bar{p}_1) \sum_{m=0}^{k-2} \bar{p}_1^m \bar{p}_2^{k-2-m} = \frac{r_0 \bar{x}_0}{r_2} 2^{k-1} (1 - \bar{p}_1) \frac{\bar{p}_1^{k-1} - \bar{p}_2^{k-1}}{\bar{p}_1 - \bar{p}_2}, \tag{72}$$

$$X_{3}^{(K)} = \frac{2r_{2}(1-\bar{p}_{2})}{d_{3}} \sum_{k=1}^{K} X_{2,k} = \frac{2r_{0}\bar{x}_{0}(1-\bar{p}_{1})(1-\bar{p}_{2})}{d_{3}} \frac{2(\bar{p}_{1}-\bar{p}_{2})+(2\bar{p}_{2})^{K}(1-2\bar{p}_{1})-(2\bar{p}_{1})^{K}(1-2\bar{p}_{2})}{(\bar{p}_{1}-\bar{p}_{2})(1-2\bar{p}_{1})(1-2\bar{p}_{2})}. (73)$$

For the total populations of the two middle compartments, we have

$$X_1^{(K)} = \sum_{k=1}^K X_{1,k} = \frac{r_0 \bar{x}_0}{r_1} \frac{1 - (2\bar{p}_1)^K}{1 - 2\bar{p}_1}, \tag{74}$$

$$X_2^{(K)} = \sum_{k=1}^K X_{2,k} = \frac{r_0 \bar{x}_0 (1 - \bar{p}_1)}{r_2} \frac{2(\bar{p}_1 - \bar{p}_2) + (2\bar{p}_2)^K (1 - 2\bar{p}_1) - (2\bar{p}_1)^K (1 - 2\bar{p}_2)}{(\bar{p}_1 - \bar{p}_2)(1 - 2\bar{p}_1)(1 - 2\bar{p}_2)}. (75)$$

Since both $2\bar{p}_1 < 1$ and $2\bar{p}_2 < 1$, we have

$$\lim_{K \to \infty} X_1^{(K)} = X_1, \quad \lim_{K \to \infty} X_2^{(K)} = X_2, \quad \lim_{K \to \infty} X_3^{(K)} = X_3,$$

see equations (20-21). Figure S13(a) shows the equilibrium values in different replication classes, $X_{1,k}$ and $X_{2,k}$. The total equilibrium populations of the four compartments (equations (74-75)) are shown in figure S13(b), as functions of the total number of replication classes, K. We observe that they converge to the values obtained previously for the system in the absence of replication classes. The convergence for $X_1^{(K)}$ is faster than that for $X_2^{(K)}$, as the latter is defined by $2\bar{p}_2 > 2\bar{p}_1$. The equilibrium values of the compartment sizes increase with K, the total number of replication classes, see figure S13(b). If the number of replication classes is greater than about 100, the system can achieve amplification for the cell numbers of increasing degrees of differentiation.

To ensure the match of system (68–69) under a specific choice of feedback on self-renewal probability, $p_i(x_0, \ldots, x_3)$, we use equations (23), where $X_1 = \sum_{k=1}^K X_{1,k}$ and $X_2 = \sum_{k=1}^K X_{2,k}$. For the numerical examples below we used the specific form of control, $p_i = c_i/(1 + h_i(x_i + y_i))$ (the "self" type). In this case, equations (23) yield:

$$c_i = \bar{p}_i(1 + h_i X_i), \quad 0 \le i \le n - 1.$$

4.2 Co-dynamics of wild-type and mutant cells.

In order to include mutations, denote by y_0 , $y_{1,k}$, $y_{2,3}$ and y_3 (with k enumerating the replication classes as before) the populations of the different types of mutants. We can write a cascade of equations for the mutants, which is similar to that of the wild-types (equations (68-69)), coupled through both the process of mutations and the self-renewal probabilities, which are functions of both wild-type and mutant populations. If a mutation occurs in compartment C_0 , we observe patterns similar to those described previously: any advantageous mutant will displace wild-type cells in compartment C_0 and consequently, in the whole lineage. It is more interesting to consider mutant generation in the downstream compartments.

For this purpose, it is convenient to ignore de-novo mutations. The equations for the wild-type cells remain the same as (68-69), except now

 $p_i = p_i(x_0, \dots, x_3, y_0, \dots, y_3)$. The equations for the mutant cells look similar, except they contain information about the difference between mutant and wild-type kinetics. We will consider several types of mutations.

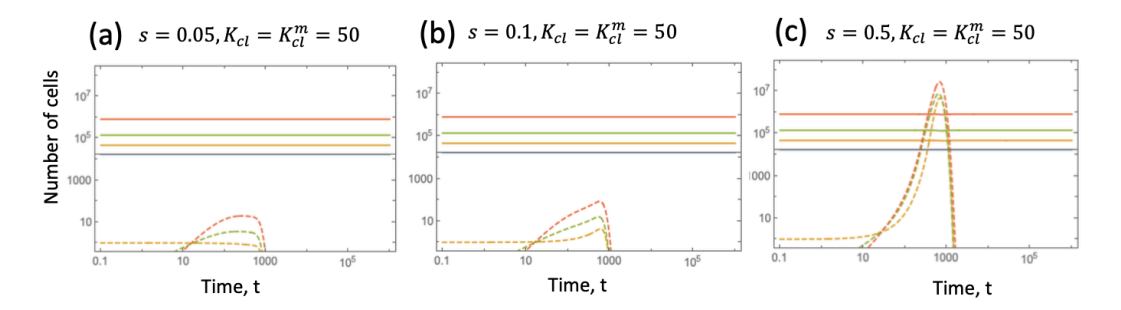


Figure S14: Mutant and wild-type dynamics for the system with replication limits, where mutations do not affect replication limits: the role of fitness advantage. The initial conditions are given by equations (70-73) for the wild-types, and all the mutant classes are zero except $y_{1,1}(0) = 1$. Total populations x_i and y_i , $0 \le i \le 3$, are plotted as functions of time. Wile-type (mutant) numbers are shown by solid (dashed) lines in compartment C_0 (blue), C_1 (yellow), C_2 (green), and C_3 (red). (a) s = 0.05, (b) s = 0.1, (c) s = 0.5. Under the "self" feedback model, $h = 10^{-9}$, u = 0, K = 50, and the rest of the parameters are as in table 1 of the main text.

Mutations that do not affect the replication capacity. Let us assume that as before, mutations affect only the self-renewal probabilities of the cells, which is reflected in the factor 1 + s. From studying the system in the absence of replication limits, we learned that mutants cannot rise if their fitness advantage, s, is below a threshold, specific to the compartment of origin. We also know that once s is above the threshold, the rise of the mutant population occurs faster for larger values of s.

These patterns remain in the system with replication limits, but there is in additional factor that plays a role in mutant dynamics. Mutants that originate in any upstream compartment, have a finite life-span during which they can rise, and once their replication capacity is exhausted, they are removed from the system. Therefore, any rise/domination of mutants can only occur for a limited amount of time. There is no steady state where mutants prevail, in the absence of mutant cells residing in C_0 .

As a result, the mutants' ability to make an impact on the system depends on their ability to rise to significant numbers, before they are wiped out due to reaching the replication capacity. Figure S14 demonstrates this by plotting the numbers of both wild-type (solid lines) and mutant (dashed lines) cells in a system with replication capacity K=50, where initially, a single mutant cell is introduced in compartment C_1 (type $y_{1,1}$). All the parameters are the same for the three panels except for the mutant fitness parameter, s. In panel (a), the mutant fitness advantage s is below the invasion threshold ($s < s_c^{(1)} \approx 0.058$), resulting in the number of mutants in C_1 declining. Note that before all mutants die out, they give rise to a certain number of cells in the downstream compartments, but being below the threshold prevents the mutant from expansion. In panel (b), the mutant fitness is above the threshold, but the time before the replication capacity of mutants is exhausted is too short for the mutants to make a significant impact. In panel (c), the mutant fitness is significantly higher and they rise much faster, such that they reach large numbers before they are wiped out.

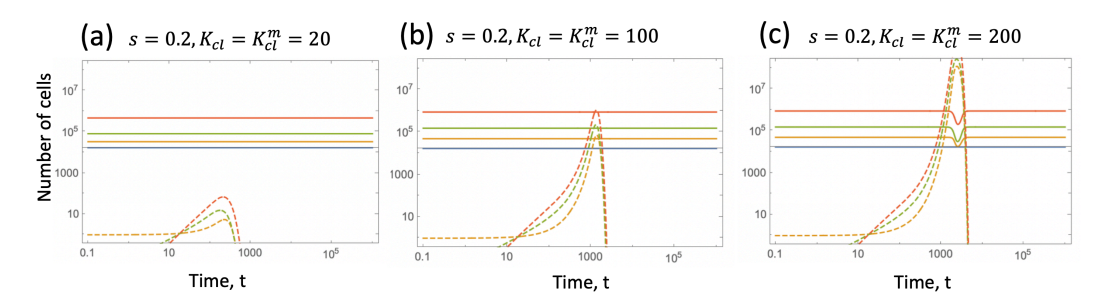


Figure S15: Mutant and wild-type dynamics for the system with replication limits, where mutations do not affect replication limits: the role of the replication limits. (a) K = 20, (b) K = 100, (c) K = 200. In all panels, s = 0.2. Notations and the rest of the parameters are as in figure S14.

In contrast to figure S14, in figure S15 the mutant fitness parameter, s, is kept constant, but the replication capacity of all cells is varied. The larger the replicative capacity, the longer is the time period during which the mutants can expand. In all panels of figure S15, we have $s > s_c^{(1)}$, and the replication capacity takes values K = 20, K = 100, and K = 200 in panels (a)-(c), respectively. The mutant's impact is the highest in panel (c), where it has a chance to rise to significant levels before crashing to zero.

Mutations that do affect the replication capacity. If the mutations are assumed to increase the replication capacity of the cells, the time during

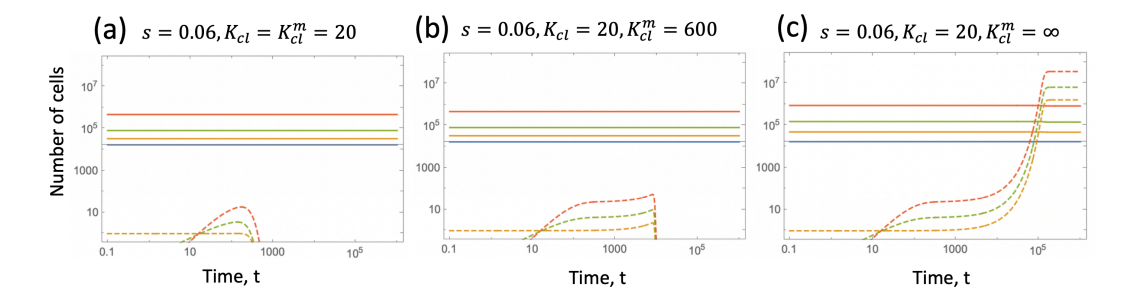


Figure S16: Mutant and wild-type dynamics for the system, where mutations affect both self-renewal probability and the replication limits. (a) $K_m = 20$, (b) $K_m = 600$, (c) $K_m = \infty$. In all panels, s = 0.06 and K = 20. Notations and the rest of the parameters are as in figure S14.

which they can expand increases, and therefore the maximum level achieved by the mutants also increases. In figure S16, the carrying capacity of the wild-type cells is kept at K=20, and mutants are just above the invasion threshold (s=0.06). In panel (a), the mutants do not have an increased replication limit, and disappear before having a chance to expand. In panel (b), the replication capacity of mutants is increased with respect to that of the wild-types, resulting in a longer mutant presence. In panel (c) we assume that mutants can divide indefinitely, and observe the establishment of a mutant steady state.

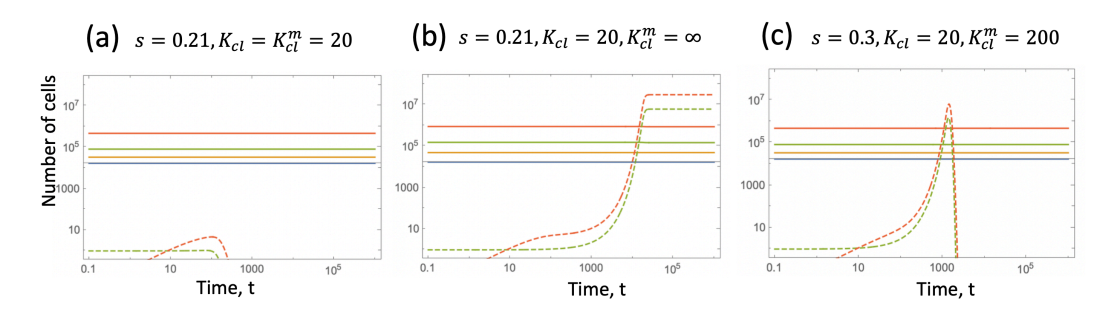


Figure S17: Similar to figures S14 S15 and S16 but the mutant originates in compartment C_2 . Initially, all the mutant classes are zero except $y_{2,2}(0) = 1$. (a) $s = 0.21, K = K_m = 20$, (b) $s = 0.21, K = 20, K_m = \infty$, (c) $s = 0.3, K = 20, K_m = 200$. Notations and the rest of the parameters are as in figure S14.

The same trends are observed if the mutant is introduced in compartment

 C_2 instead of C_1 . In figure S17, a mutant generated in C_2 with the fitness advantage just above the threshold $(s = 0.21 > s_c^{(2)} \approx 0.203)$ does not have a chance to rise if the replication capacity is low (panel (a)), but increasing the mutants' carrying capacity $(K_m = \infty \text{ in panel (b)})$ leads to the establishment of a mutant equilibrium. In panel (c), the mutant's fitness advantage, s, is higher, such that it rises to significant levels even under a finite replicative capacity $(K_m = 200)$, before being flushed out of the system.

References

- [1] Katrin Busch, Kay Klapproth, Melania Barile, Michael Flossdorf, Tim Holland-Letz, Susan M Schlenner, Michael Reth, Thomas Höfer, and Hans-Reimer Rodewald. Fundamental properties of unperturbed haematopoiesis from stem cells in vivo. *Nature*, 518(7540):542–546, 2015.
- [2] Munetomo Takahashi, Melania Barile, Richard H Chapple, Yu-jung Tseng, Daisuke Nakada, Katrin Busch, Ann-Kathrin Fanti, Petter Säwén, David Bryder, Thomas Höfer, et al. Reconciling flux experiments for quantitative modeling of normal and malignant hematopoietic stem/progenitor dynamics. Stem cell reports, 16(4):741–753, 2021.